Supporting Information

Strategies for enhancing the processability of UHMWPE

Clement G. Collins Rice,[ab] Alexander Evans,[a] Zoë R. Turner,[a] Jirut Wattoom,[bc] and Dermot O'Hare*[a]

[a] Chemistry Research Laboratory, University of Oxford, 12 Mansfield Road, Oxford, OX1 3TA, United Kingdom.
[b] SENFI UK Ltd., Centre of Innovation and Enterprise, Begbroke Science Park, Woodstock Road, Begbroke, OX5 1PF, United Kingdom.
[c] SCG Chemicals PLC, 1 Siam Cement Road, Bangsue, Bangkok 10800, Thailand.

Table of Contents

1 Synthesis and characterisation of UHMWPE

Synthesis and characterisation of UHMWPE. UHMWPE was synthesised using $\mathbf{1}_{\mathbf{sMAO}(200)}$ at a polymerisation temperature (T_p) of 60 °C under 2 bar ethylene pressure, with hexane as a diluent and Al^iBu_3 (TIBA) as cocatalytic scavenger. Relatively stable reaction kinetics were observed (Figure S2) with at most a moderate decay in activity up to 2 hours (2190 kg_{PE} mol_{Ti}^{-1} h^{-1} bar^{-1}). It was shown that reducing the concentration of TIBA scavenger from 72 mM to 1.8 mM did not result in a meaningful change in catalytic activity but effected an increase in molecular weight from 1.7 MDa to 2.7 MDa (Figure S3).

For bulk characterisation, several batches (2 hours, [TIBA] = 15 mM) were combined to give a total polymer yield of 61 g. The molecular weight was determined by gel permeation chromatography (GPC) to be M_w = 3.4 MDa, with $Đ$ = 4.1 (Figure S1). The UHMWPE was pressed into a plate at 180 °C, from which was cut ISO type 5A test specimens. Density, ρ, was determined according to ISO1183-1 and was found to be 930 kg m^{-3}. Tensile measurements were performed according to ISO527-1/-2 (Figure S14). The Young's modulus, E, was measured as 0.627 GPa, with an ultimate tensile strength, σ_B, of 50.9 MPa at a strain, ε_B, of 198%. A yield point, σ_y, is seen between 19.5–22.0 MPa and strain hardening is observed $\varepsilon > \varepsilon_y$. These values are all in the range of commercially available UHMWPEs (average values: ρ = 951 kg m^{-3}, E = 0.715 GPa, σ_B = 36.5 MPa, ε_B = 244%, σ_y = 19.3 MPa).[1]

Determination of molecular weight. Due to the high viscosity of high molecular weight polymer solutions, the estimation of M_w by GPC becomes less reliable as M_w increases.[2] Melt-phase small-amplitude oscillatory shear (SAOS) rheometry was performed to confirm the ultra-high molecular weight, and additionally assess entanglement density. The polymer was pressed into a disc, and heated to 160 °C in the rheometer, well above the T_m. Following equilibration, a frequency sweep was performed from 10^{-2} to 10^2 rad s^{-1}, with the viscoelastic response measured (Figure S10). Upon application of a shear force, the energy is partially stored elastically in the melt (storage modulus, G'), with the remainder lost as heat through viscous flow (loss modulus, G''). Taken together, this technique allows for the full characterisation of the flow behaviour of a melt, crucial for determining industrial processability. The UHMWPE melt shows an extremely high melt viscosity, $|\eta^*|$, above 10^8 Pa·s at low ω, but demonstrates a degree of shear-thinning, reducing below 10^4 Pa·s at high ω. This is substantially greater than a commercial Ziegler-Natta HDPE (SCG Chemicals PLC; M_w = 225 kDa; $Đ$ = 25) which was found to have $|\eta^*|$ on the order of 10^4 Pa·s (10^{-2} rad s^{-1}) to 10^2 Pa·s (10^2 rad s^{-1}). The frequency-domain crossover point (ω_c) of storage and loss moduli is related to the molecular weight, with a lower crossover frequency corresponding to higher molecular weight. Using UHMWPEs with narrow dispersity, Talebi *et al.* used a "modulus model" to show that $\omega_c = 10^{-3}$ rad s^{-1} corresponded to a polymer having a molecular weight around 3 MDa.[3] Static stress-relaxation time-domain experiments, Fourier transformed into the frequency-domain, were utilised to extend the range of measurement as low as 10^{-7} rad s^{-1} in order to determine the crossover point of UHMWPEs – a value of ω_c around 10^{-5} rad s^{-1} corresponded to a polymer sample having a molecular weight around 10 MDa, despite being measured by GPC at 5.7 MDa. This highlights the limitations of GPC for the determination of extremely high molecular weights, and the advantages of rheological techniques combined with detailed physical modelling. Gote *et al.* found that a crossover point of 10^{-2} and 10^{-3} rad s^{-1} related to a polymer having M_w of 1 and 2 MDa respectively, consistent with the work of Talebi *et al.*.[4] In the current work, utilizing time-domain creep compliance results Fourier transformed into the frequency domain ($\mathcal{F}[J(t)] \rightarrow G^*(\omega)$),[5] the rheological crossover point is found

to be between 2–4 x 10^{-4} rad s^{-1}. A M_w of 4–5 MDa is therefore plausible, within the region estimated by high-temperature GPC, or at most slightly greater.

Disentanglement. A key characteristic of UHMWPE is the entanglement density. "Disentangled" UHMWPE (*dis*UHMWPE), has an entanglement density in the amorphous region sufficiently low to allow processing in the solid state below T_m, thus overcoming many of the processability challenges that result from the extremely high intrinsic viscosity.[6-11] The entangled state is the entropically-driven thermodynamically favoured state, and thus *dis*UHMWPE, heated above its T_m, reverts to an entangled state.[12] Observing the formation of the entangled state is therefore direct evidence for nascent disentanglement in the sample. A DSC annealing protocol has previously been used to suggest a degree of nascent disentanglement in UHMWPE synthesized by PHENI* catalysts supported on sMAO.[13] The DSC methodology has been established by Rastogi *et al.* among others: during annealing, sequential chain detachment from the disentangled lamellae results in the formation of two melting peaks on a subsequent heating cycle – the melt-crystallised fraction and the remaining nascent fraction.[6,7,14-18]

Very recently, work by Litvinov *et al.* has cast doubt on the existence of a metastable non-equilibrium disentangled melt.[19] Entropy-driven chain explosion results in local re-entanglement in the melt over the course of a few nanoseconds, with topological knots forming a uniform distribution over a long time by chain reptation. Utilising ^{1}H NMR relaxometry, the authors reported the near-instantaneous re-entangling of solution-crystallised UHMWPEs, with no measurable difference between nascent disentangled and entangled samples. This field remains controversial, with the determination of entanglement density in nascent powders proving complex and challenging.

Time-domain rheometry was used to further probe the entanglement density (Figure S11), since the storage modulus and the molecular weight between entanglements (M_e) are related through $\langle M_e \rangle = \rho RT/G_0$.[17] Under a shear force, more energy can be stored in an entangled polymer than disentangled by virtue of the entanglements acting as physical crosslinks with elastic properties. Since the equilibrium entangled state therefore has a higher storage modulus, G', than the nascent disentangled state, the build-up of storage modulus over time has been shown to correlate with the degree of entanglement.[20,21] The nascent sample of UHMWPE synthesised by $\mathbf{1}_{\mathbf{sMAO}(200)}$/TIBA shows G' increasing over a long timescale, having not reached a completely flat plateau even after 10^5 s (27 hours). This compares against the commercial Ziegler-Natta UHMWPE (entangled; M_w = 4.5 MDa, $Đ$ = 31) studied by Liu *et al.* which reaches a plateau of 1.45 MPa after approximately 5 minutes, having had an initial G' value of 1.40 MPa, in contradistinction to their *dis*UHMWPE (M_w = 4.8 MDa, $Đ$ = 3.1) which increased from an initial value of 0.65 MPa to reach a plateau at 1.9 MPa after 18 hours.[12] In the current work, the particularly low initial G' of 0.14 MPa, and the increase observed over very long timescales is strong evidence, when combined with previously-reported DSC annealing protocols,[13] for a low entanglement density in the nascent polymer produced by the PHENI* catalyst.

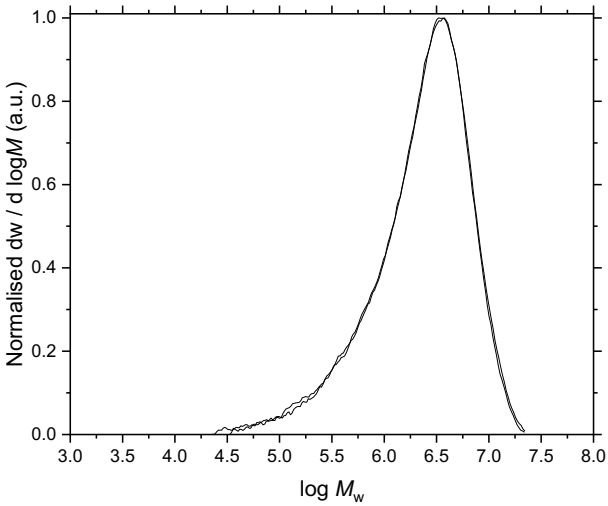

Figure S1 Gel-permeation chromatogram of polyethylene synthesised by **1**$_{sMAO}$. Polymerization conditions: Polymerisation conditions: 10 mg solid catalyst, 150 or 750 mg TIBA, 2 bar ethylene, 50 or 250 mL hexanes, and 60 °C. Two parallel measurements shown to demonstrate sample homogeneity.

1.1 Kinetics

Table S1 Polymerisation conditions: $[Al_{sMAO}]_0/[Ti]_0$ = 200, 10 mg catalyst, 2 bar ethylene, 50 or 250 mL hexanes, 60 °C, and 150 or 750 mg TIBA.

Catalyst	T_p /°C	Solvent /mL	Time /minutes	Activity /kg mol$_{Ti}^{-1}$ h^{-1} bar^{-1}	M_w /kDa	Đ
1$_{sMAO}$	60	50	5	7000 ± 220	1942	6.4
1$_{sMAO}$	60	50	15	5190 ± 210	2430	5.3
1$_{sMAO}$	60	50	30	3720 ± 110	2088	5.2
1$_{sMAO}$	60	50	60	2780 ± 420	2776	4.8
1$_{sMAO}$	60	50	120	2190 ± 50	3198	3.7
1$_{sMAO}$	60	250	5	6850	2285	2.4
1$_{sMAO}$	60	250	120	2460	2221	2.3

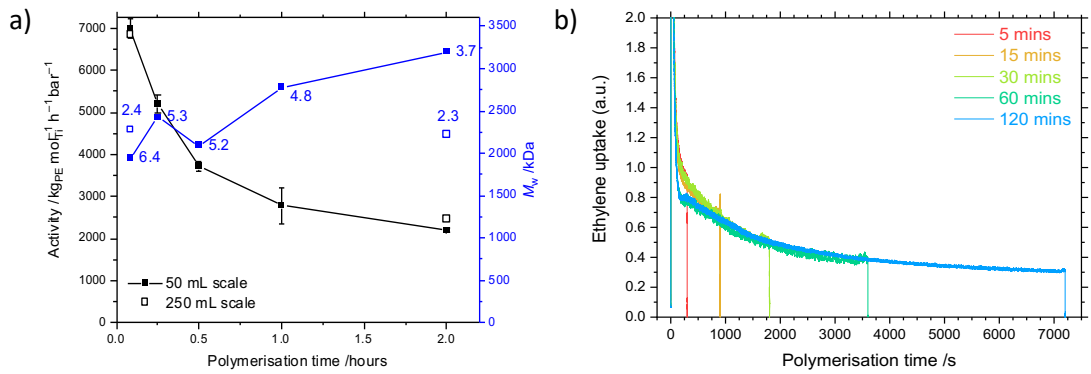

Figure S2 a) Slurry-phase mean polymerisation activity and polymer molecular weight (M_w, Đ annotated), and b) ethylene uptake as a function of reaction time using **1**$_{sMAO}$. Polymerisation conditions: 10 mg solid catalyst, 150 or 750 mg TIBA, 2 bar ethylene, 50 or 250 mL hexanes, and 60 °C. Error bars shown at one standard deviation.

1.2 Cocatalyst loading

Table S2 Polymerisation conditions: $[Al_{sMAO}]_0/[Ti]_0$ = 200, 10 mg catalyst, 2 bar ethylene, 50 mL hexanes, 60 °C, 30 minutes.

Catalyst	T_p /°C	[TIBA] /mM	$[TIBA]_0/[Ti]_0$	Activity /kg mol_{Ti}^{-1} h^{-1} bar^{-1}	M_w /kDa	Đ
1_{sMAO}	60	0	0	240 ± 20	1695	3.7
1_{sMAO}	60	1.8	125	3970 ± 420	2654	6.9
1_{sMAO}	60	3.6	250	4020 ± 40	2807	3.3
1_{sMAO}	60	7.2	500	4330 ± 180	2330	6.4
1_{sMAO}	60	15.1	1059	3720 ± 110	2088	5.2
1_{sMAO}	60	35.8	2500	3830 ± 160	1853	7.3
1_{sMAO}	60	71.5	5000	3680 ± 80	1671	6.8

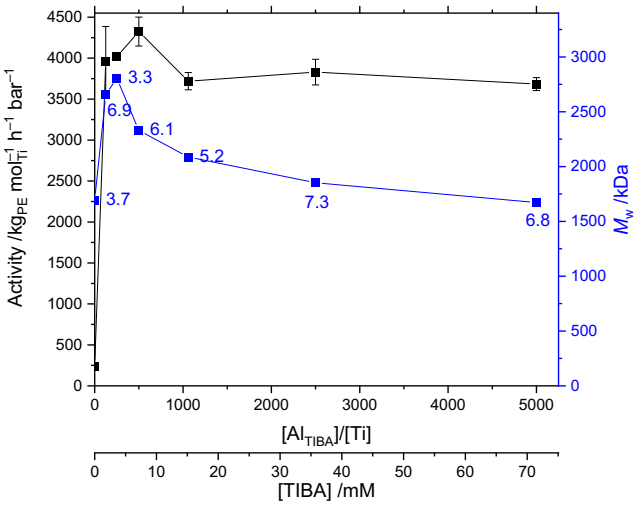

Figure S3 Slurry-phase mean polymerisation activity and polymer molecular weight (M_w, Đ annotated) as a function of $[Al_{TIBA}]/[Ti]$ using **1_{sMAO}**. Polymerisation conditions: 10 mg solid catalyst, 2 bar ethylene, 50 mL hexanes, 60 °C, and 30 minutes. Error bars shown at one standard deviation.

1.3 Scale

Table S3 Polymerisation conditions: $[Al_{sMAO}]_0/[Ti]_0$ = 200, 150 mg TIBA, 2 bar ethylene, 50 mL hexanes, 60 °C, and 30 minutes.

Catalyst	Temperature /°C	Catalyst mass /mg	Activity /kg mol_{Ti}^{-1} h^{-1} bar^{-1}	M_w /kDa	Đ
1_{sMAO}	60	5	3400 ± 3	2575	4.3
1_{sMAO}	60	10	3720 ± 110	2088	5.2
1_{sMAO}	60	15	3020 ± 500	1950	5.7
1_{sMAO}	60	20	2780 ± 7	1872	5.9

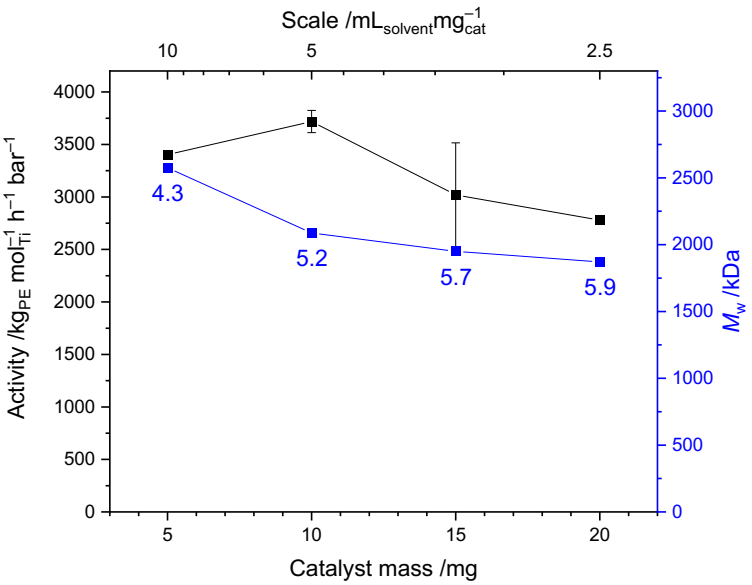

Figure S4 Slurry-phase mean polymerisation activity and polymer molecular weight (M_w, $Đ$ annotated) as a function of catalyst loading (reaction scale) using **1**$_{sMAO}$. Polymerisation conditions: 150 mg TIBA, 2 bar ethylene, 50 mL hexanes, 60 °C and 30 minutes. Error bars shown at one standard deviation.

1.4 Gel-permeation chromatography

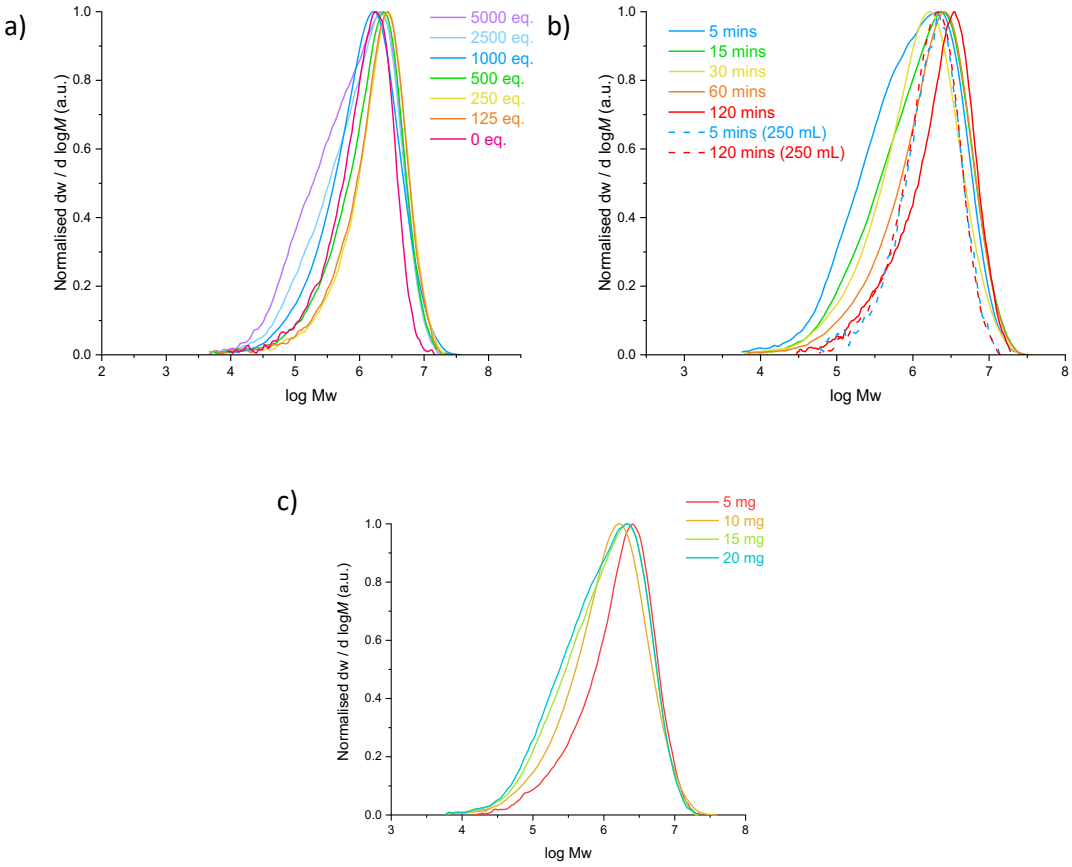

Figure S5 Gel-permeation chromatograms of polyethylene produced by $\mathbf{2}_{\mathbf{sMAO}}$ as a function of a) [TIBA][Ti], b) time or c) catalyst amount. Polymerisation conditions: 5–20 mg catalyst, 2 bar ethylene, 50–250 mL hexanes, 5–120 minutes, 150–750 mg TIBA, and 60 °C.

1.5 Differential scanning calorimetry

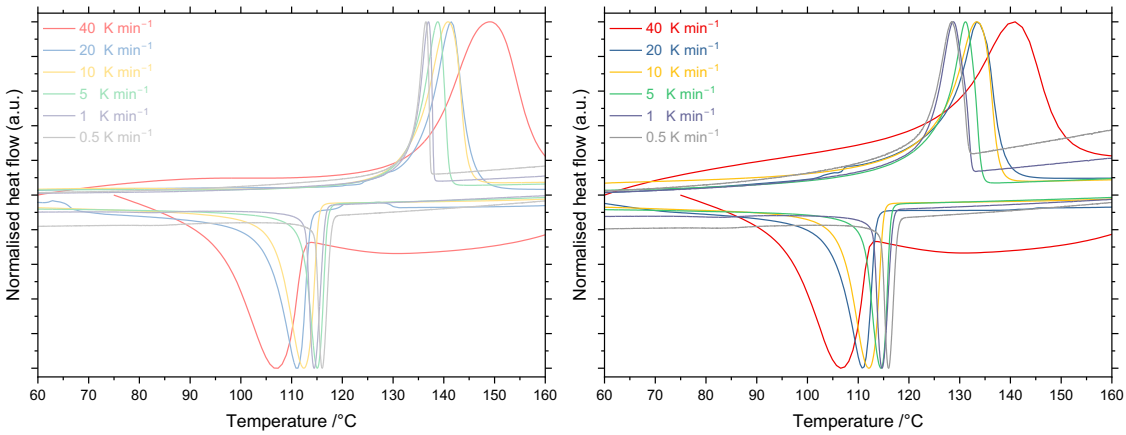

Figure S6 Differential scanning calorimetry plot of polyethylene produced by $\mathbf{1}_{\mathbf{sMAO}}$/TIBA at varying heating rates (0.5–40 K min^{-1}; left: first heating cycles; right: second heating cycle). Polymerisation conditions: 10 mg catalyst, 150 mg TIBA, 2 bar ethylene, 50 mL hexanes, and 60 °C.

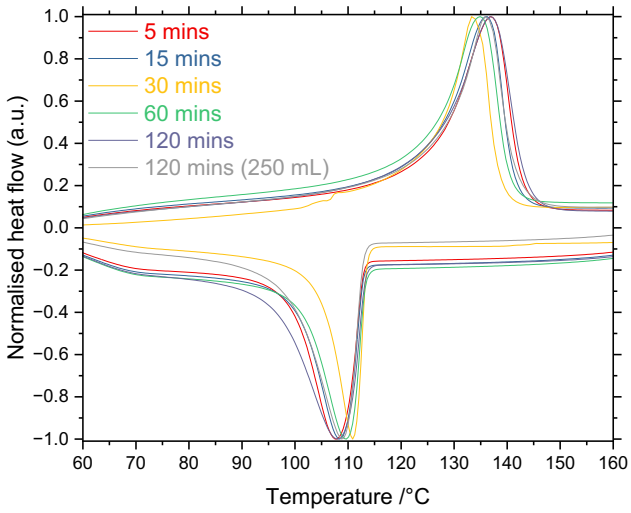

Time /minutes	T_m /°C	Xc (%)
5	136.8	79.8
15	136.2	72.6
30	133.4	77.7
60	134.9	77.9
120	137.1	72.5
120 (250 mL)	136.0	66.6

Figure S7 Differential scanning calorimetry plot of polyethylene produced by $\mathbf{1}_{sMAO}$/TIBA as a function of time. Polymerisation conditions: 10 mg catalyst, 150 or 750 mg TIBA, 2 bar ethylene, 50 or 250 mL hexanes, and 60 °C.

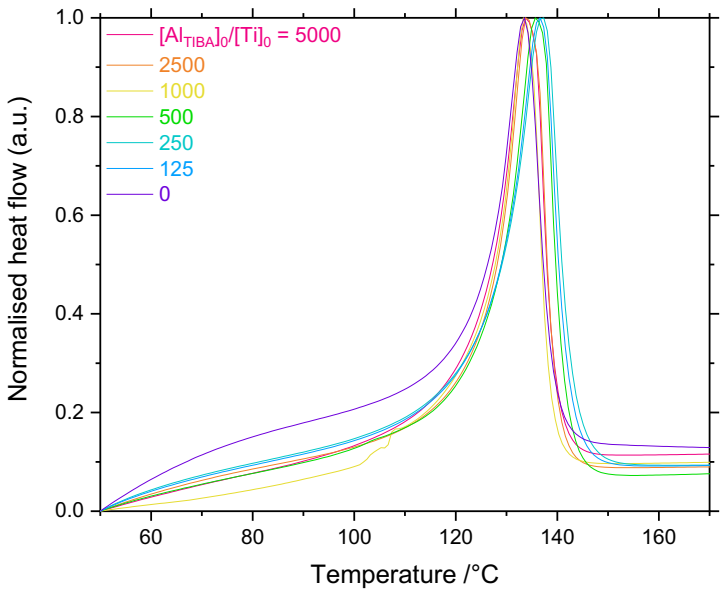

[Al$_{TIBA}$]/[Ti]	T_m /°C	X_c (%)
5000	133.9	72.6
2500	134.0	69.7
1000	133.4	77.7
500	135.9	56.6
250	137.1	65.6
125	136.6	64.0
0	133.5	66.6

Figure S8 Differential scanning calorimetry plot of polyethylene produced by $\mathbf{1}_{sMAO}$/TIBA as a function of [Al]/[Ti]. Polymerisation conditions: 10 mg catalyst, [TIBA]/[Ti] = 0–5000, 2 bar ethylene, 50 mL hexanes, 30 minutes, and 60 °C.

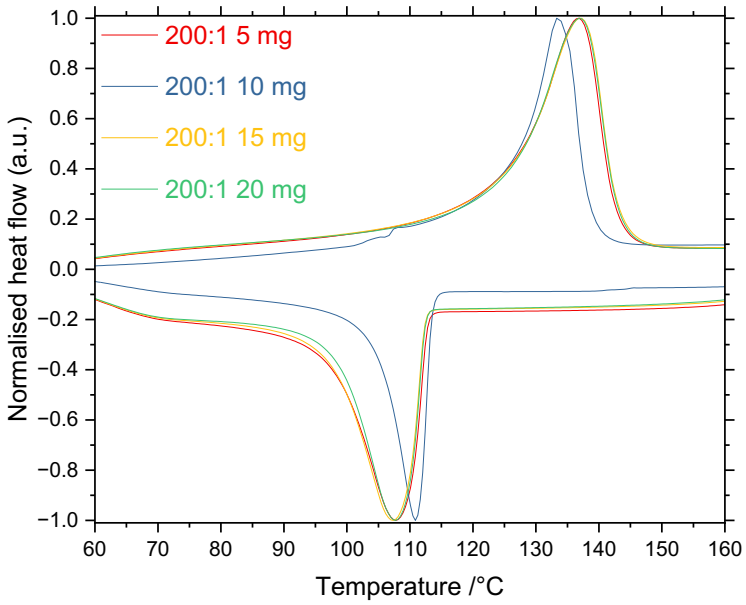

Mass /mg	T_m /°C	X_c (%)
5	136.7	74.2
10	133.4	77.7
15	137.0	75.1
20	137.1	83.9

Figure S9 Differential scanning calorimetry plot of polyethylene produced by $\mathbf{1}_{\mathbf{sMAO}}$/TIBA as a function of catalyst loading (reaction scale) using $\mathbf{1}_{\mathbf{sMAO}(200)}$.

1.6 Rheometry

All measurements were performed at 160 °C. SAOS rheology was performed at a strain of 0.1% (within the LVE region). Strain sweep measurements were performed at ω = 10 rad s^{-1}. Creep compliance measurements were performed with stress = 6.6 x 10^3 Pa (approximately $|G^*|$ at ω = 0.01 rad s^{-1} multiplied by 0.04, as suggested by Inn and Rohlfing,[22] and transformed into the frequency domain using TRIOS®.

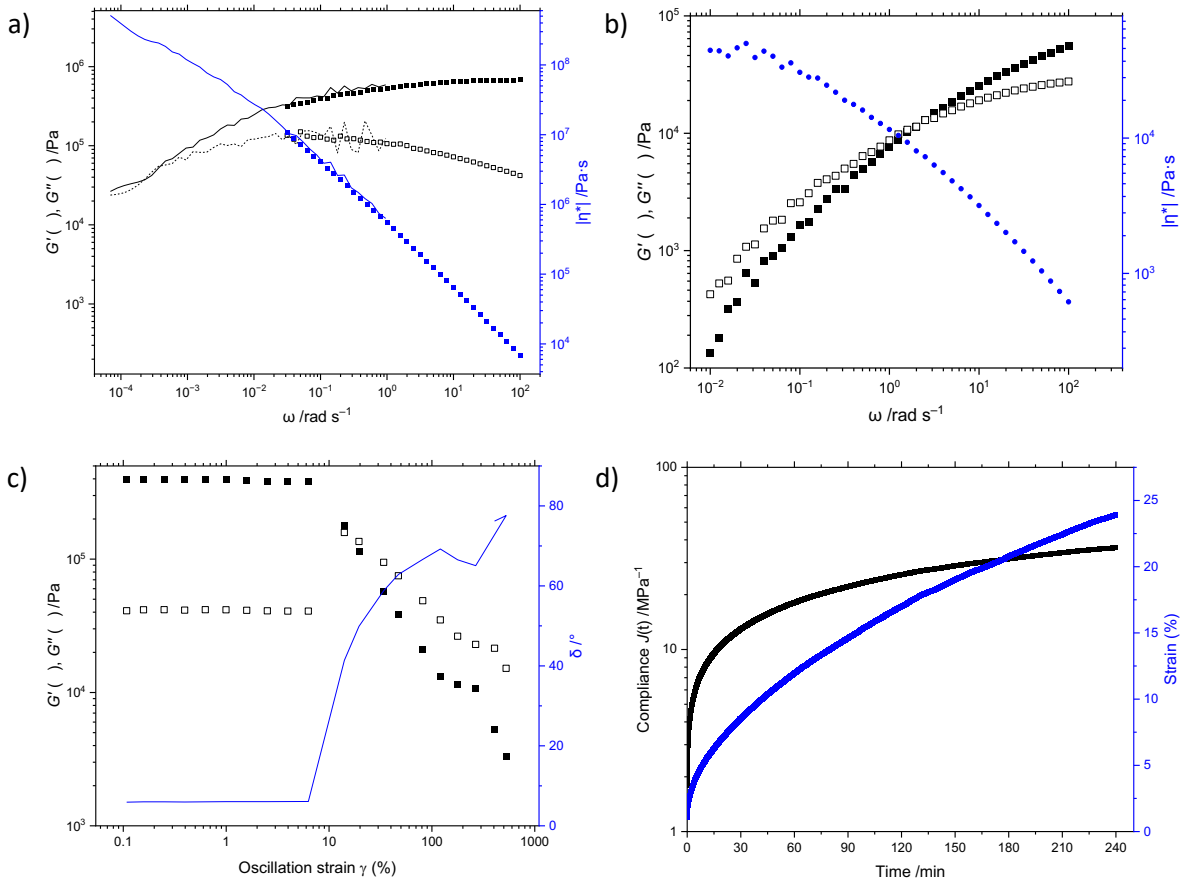

Figure S10 Frequency sweep rheometric curves measured at 160 °C for a) UHMWPE synthesised by **1**$_{sMAO}$/TIBA (M_w = 2.08 MDa, $Đ$ = 5.1; solid and dashed lines represent creep compliance results transformed into the frequency domain; modulus crossover: 4–6 x 10^4 Pa; 2–4 x 10^{-4} rad s^{-1}) and b) HDPE obtained from SCG Chemicals (M_w = 225 kDa, $Đ$ = 25; modulus crossover: 1.29 x 10^4 Pa, 2.51 rad s^{-1}). Rheology of UHMWPE c) as a function of oscillation strain (LVE region γ < *ca.* 6%), and d) creep compliance, *J*(t). Storage modulus, *G′*; loss modulus, *G′′*, complex viscosity, |η*|; angular frequency, ω; phase angle, δ. $\eta^* = \eta' + i\eta'' = \frac{G^*}{\omega}$; $\tan\delta = \frac{G'}{G''}$; $J(t) = \frac{\gamma(t)}{\sigma}$.

Time-domain oscillatory rheology was performed on nascent polymer samples (compression moulded at r.t.) with ω = 10 rad s^{-1}.

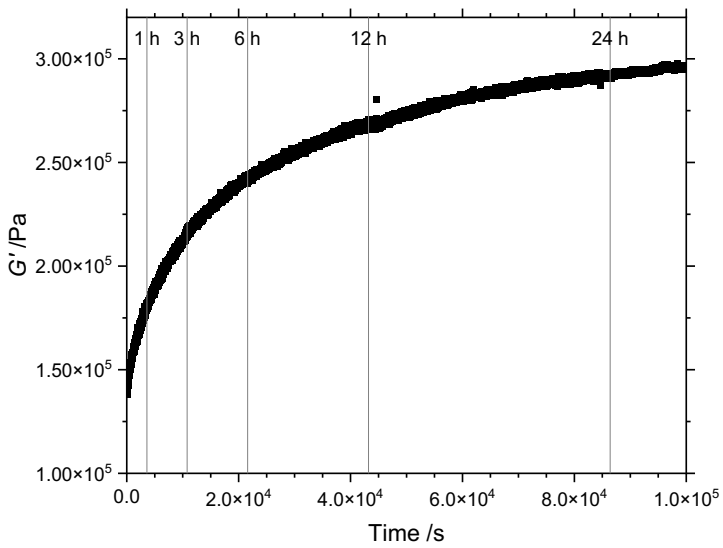

Figure S11 Time sweep rheometric curve, measured at 160 °C, of UHMWPE synthesised by $\mathbf{1}_{sMAO}$/TIBA. The build-up of storage modulus over time is evidence for nascent disentanglement.

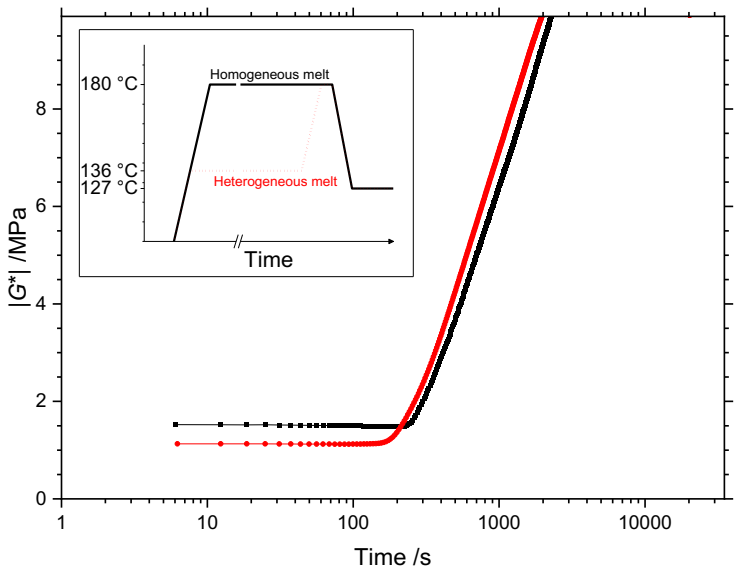

Figure S12 Isothermal crystallisation SOAS (127 °C, ω = 10 rad s^{-1}) of UHMWPE synthesised by $\mathbf{1}_{sMAO}$/TIBA following two melting protocols (inset): fast (100 minutes at 180 °C resulting in "homogeneous melt") and slow (18 hours at 136 °C resulting in "heterogeneous melt"). This follows the work of Rastogi *et al.* (*Nat. Mater.*, 2005, **4**, 635-641) who found that – for disentangled UHMWPE – the heterogeneous melt had a lower *G** and crystallised an order of magnitude faster than the homogeneous melt.[14] While a smaller effect is observed for this sample, faster melting kinetics seen under the heterogeneous protocol is consistent with higher local chain mobility and easier nucleation, in turn providing evidence for disentanglement in the nascent polymer. $G^* = G' + iG''$.

1.7 Wide-angle X-ray scattering

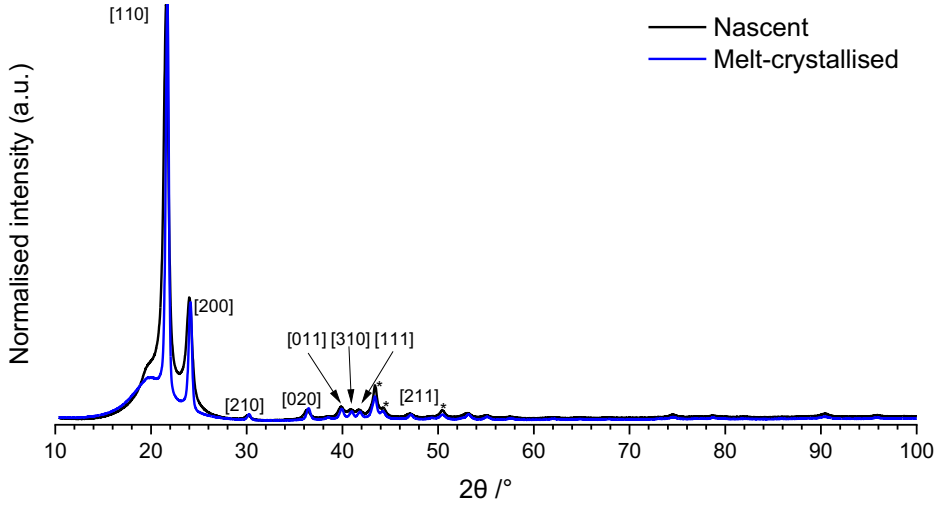

Figure S13 WAXS pattern of nascent and melt-crystallised UHMWPE. Measurements were performed using a PANAnalytical X'Pert Pro Diffractometer in scanning mode using Cu Kα radiation (1.542 Å). Sample were placed into a steel sample holder and analysed from 10 to 100 °, with a step size 0.0167 2θ and count time of 156.845 s. The sample were then heated *in vacuo* at 195 °C for 1 hour before cooling and running again under the same conditions. Reflections from the sample holder are denoted by an asterisk (*). Indexing is consistent with the findings of Cser.[23] The nascent sample has [110] reflection at 2θ of 21.599 ° and the [200] reflection at 23.989 °; following melt-crystallisation, the [110] reflection is at 2θ of 21.716 ° and the [200] at 24.122 °. Crystallinity determined from WAXS (by Lorentz fitting of the [110] and [200] peaks compared to integrating diffraction pattern between $10 \leq 2\theta/° \leq 29$) is 83% (nascent) and 67% (melt-crystallised).[24] The reduction in crystallinity is consistent with an increase in entanglement in the amorphous region, in turn providing evidence for nascent disentanglement.

1.8 Tensile testing

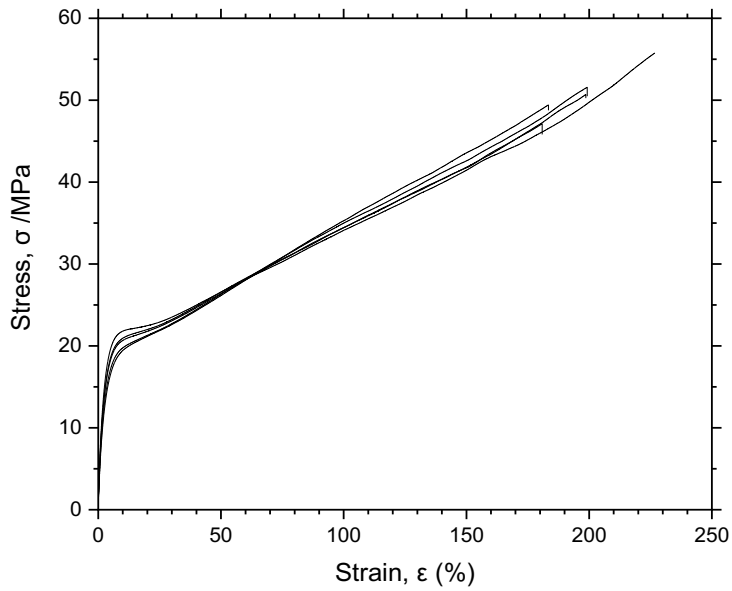

Figure S14 Engineering stress-strain tensile curves for UHMWPE synthesised by $\mathbf{1}_{\mathbf{sMAO}}$/TIBA ($N$ = 5). Strain hardening is modelled according to Hollomon's equation, $\sigma = K\varepsilon^n$, with K = 401 MPa and n = 0.47 ($0.50 < \varepsilon < 1.80$).

2 Surface concentration effects of PHENI* complex on sMAO

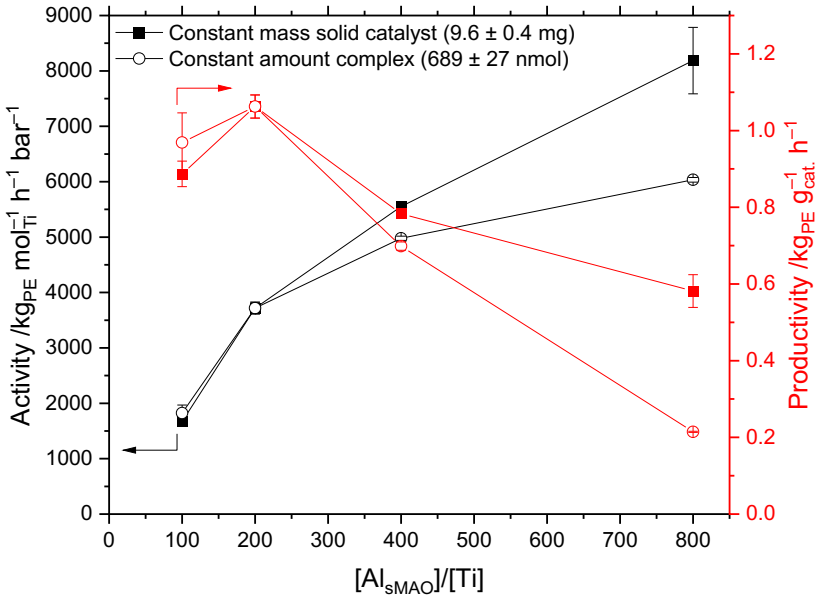

Figure S15 Slurry-phase ethylene polymerization activity and gravimetric productivity of **1$_{sMAO}$**/TIBA at T_p = 60 °C as a function of [Al$_{sMAO}$]/[Ti].

2.1 Gel-permeation chromatography

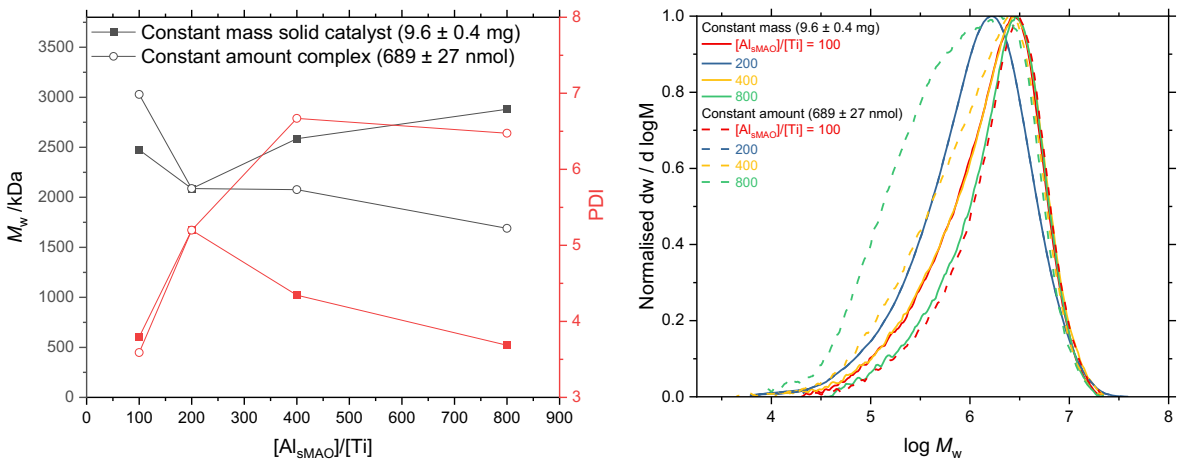

Figure S16 Weight-average molecular weight and dispersity (left), and gel-permeation chromatograms (right) of polyethylene synthesised by **1$_{sMAO}$**/TIBA of varying [Al$_{sMAO}$]/[Ti].

2.2 Differential Scanning Calorimetry

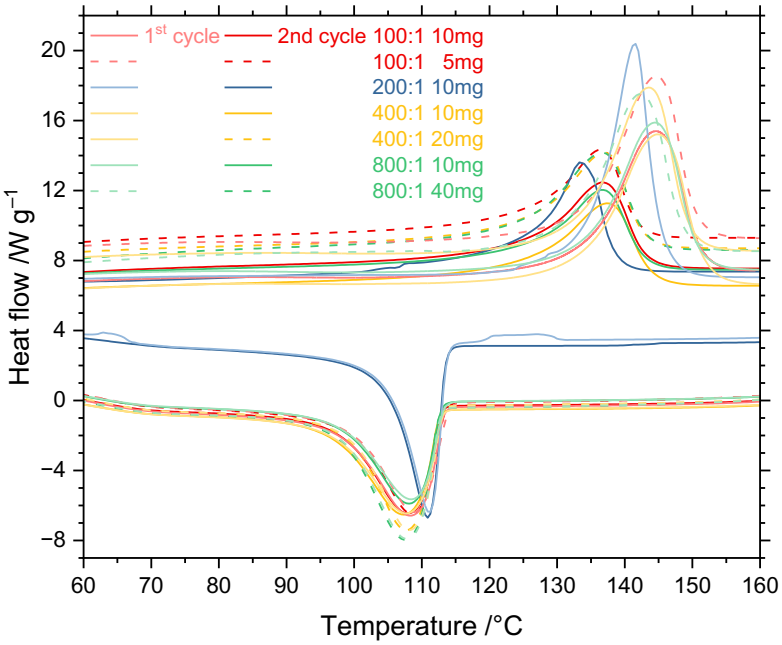

		First cycle		Second cycle	
[Al_{sMAO}]/[Ti]	Mass /mg	T_m /°C	X_c (%)	T_m /°C	X_c (%)
100	10	144.5	94	136.8	74.6
100	5	144.6	109	136.5	71.5
200	10	141.4	109	133.4	77.7
400	10	145.0	104	137.4	73.1
400	20	143.4	109	137.1	79.9
800	10	144.5	94	136.8	72.3
800	40	142.4	106	136.7	81.1

Figure S17 Differential scanning calorimetry plot of polyethylene produced by $\mathbf{1}_{sMAO}$/TIBA as a function of [Al_{sMAO}]/[Ti] and catalyst mass. Polymerisation conditions: 150 mg TIBA, 2 bar ethylene, 50 mL hexanes, 30 minutes, and 60 °C.

2.2.1 Annealing experiments

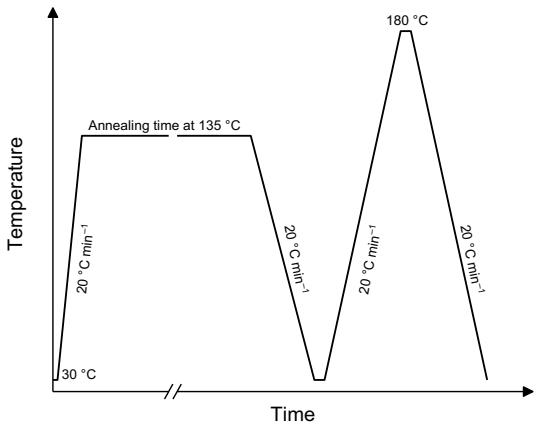

Figure S18 Graphical representation of the protocol used for DSC annealing experiments.[7]

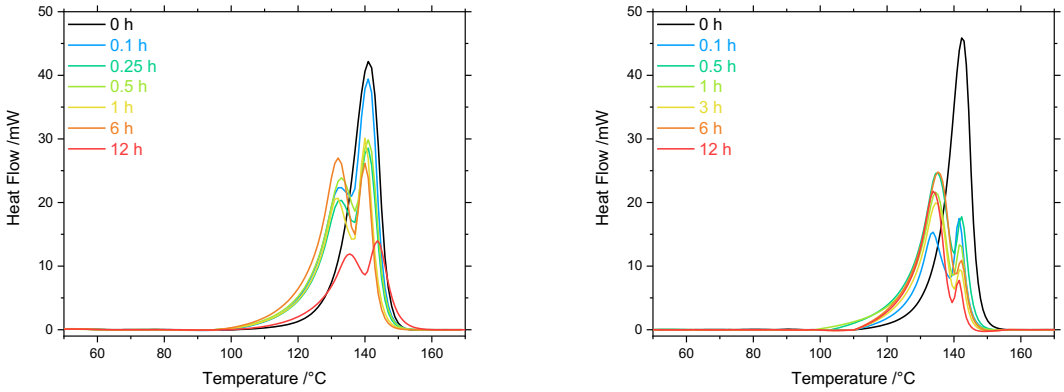

Figure S19 Differential scanning calorimetry plots of UHMWPE synthesised by $\mathbf{1}_{\mathbf{sMAO}(100)}$ (left) and $\mathbf{1}_{\mathbf{sMAO}(200)}$ (right) as a function of annealing time.

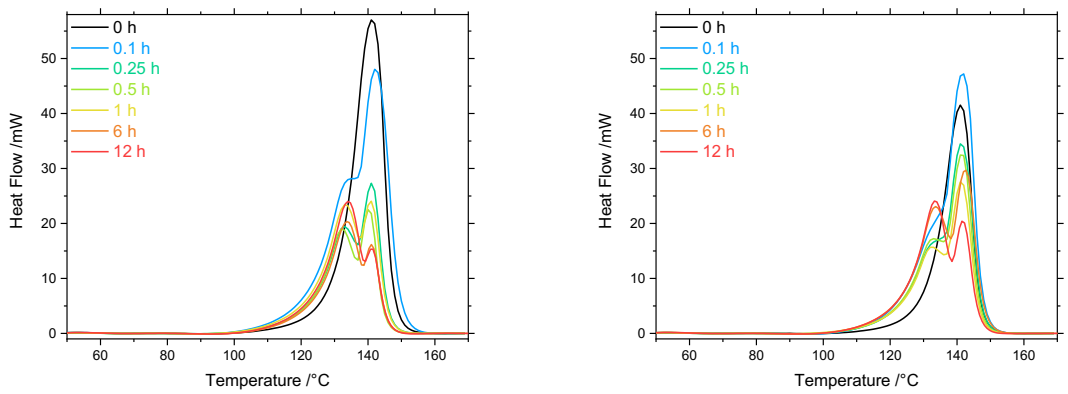

Figure S20 Differential scanning calorimetry plots of UHMWPE synthesised by $\mathbf{1}_{\mathbf{sMAO}(400)}$ (left) and $\mathbf{1}_{\mathbf{sMAO}(800)}$ (right) as a function of annealing time.

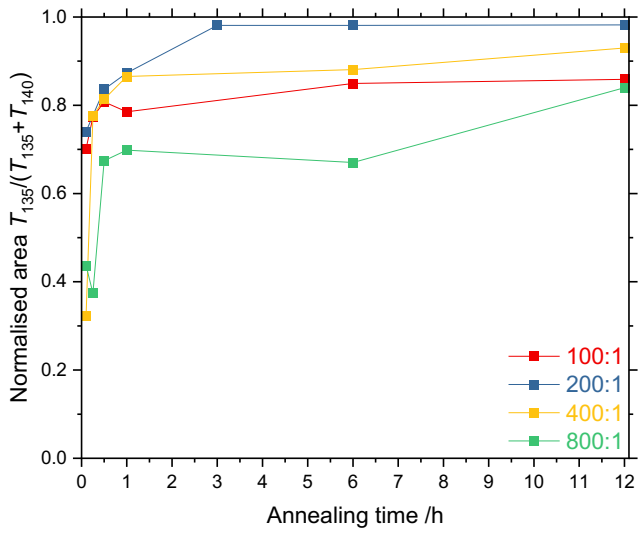

Figure S21 Normalised area $T_{135\,°C}/(T_{135\,°C}+T_{140\,°C})$ as a function of annealing time of polyethylene synthesised by $\mathbf{1_{sMAO}}$ of varying $[Al_{sMAO}]/[Ti]$.

2.3 Rheology

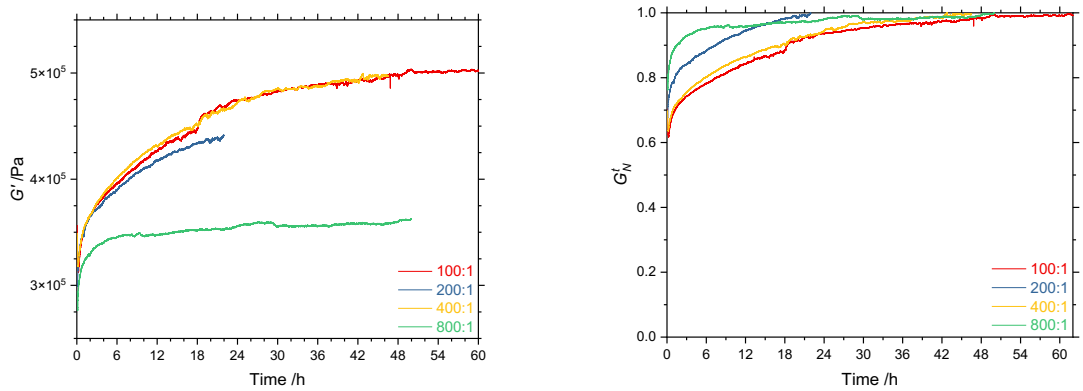

Figure S22 Storage modulus, *G'*, (left) and normalized storage modulus, G^t_N, (right) of polyethylene synthesised by $\mathbf{1_{sMAO}}$ of varying $[Al_{sMAO}]/[Ti]$ as a function of annealing time. Measured at 160 °C, with ω = 10 rad s^{-1}.

3 Chain transfer agents for broad molecular weight distributions

3.1 Hydrogen response

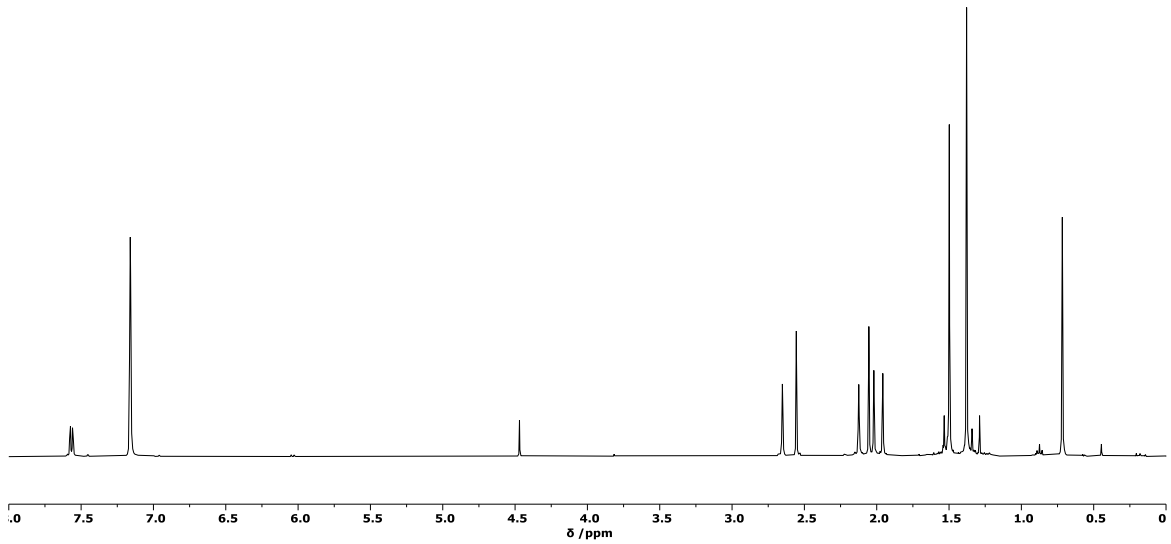

Figure S23 ^{1}H NMR spectrum (400 MHz, benzene-d_6, 300 K) of **1** with H_2 (1 bar) after heating for 1 h at 80 °C. The H_2 resonance is seen at δ 4.47 ppm, and no change is observed for the ligand resonances associated with **1**.[25] This indicates that the ligand is not prone to hydrogenolysis, and that the catalyst is expected to be stable towards hydrogen.

Table S4 Polymerisation conditions: $[Al_{sMAO}]_0/[Ti]_0$ = 200, 150 mg TIBA, 2 bar ethylene/hydrogen (98:2), 50 mL hexanes, and 30 minutes.

Catalyst	T_p /°C	Time /minutes	Activity /kg mol_{Ti}^{-1} h^{-1} bar^{-1}	M_w /kDa	Đ
$\mathbf{1}_{sMAO}$	50	30	1690 ± 240	110	9.5
	60	30	1770 ± 80	91	7.2
	70	30	1170 ± 30	110	6.9
	80	30	1160 ± 190	89	5.4
	90	30	1100 ± 240	85	4.5

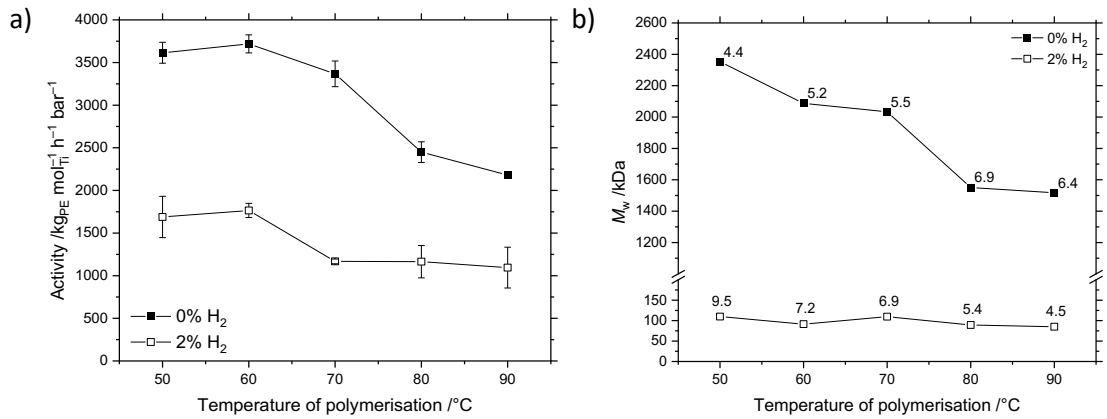

Figure S24 a) Slurry-phase mean ethylene polymerisation activity, and b) polymer molecular weight (M_w, Đ annotated) as a function of temperature for sMAO-^{Me2}SB(^{tBu2}ArO,I*)TiCl$_2$ ($\mathbf{1}_{sMAO}$) in the presence of dihydrogen. Polymerisation conditions: 10 mg solid catalyst, 150 mg TIBA, 2 bar ethylene or ethylene/hydrogen (98:2), 50 mL hexanes, and 30 minutes. Error bars shown at one standard deviation.

3.1.1 Differential scanning calorimetry

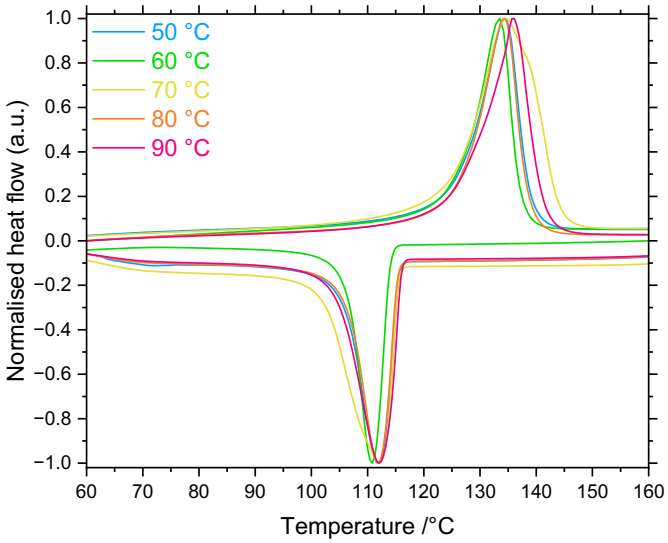

Figure S25 Differential scanning calorimetry plot of polyethylene produced by **1**$_{sMAO}$/TIBA as a function of T_p. Polymerisation conditions: 10 mg catalyst, [TIBA]/[Ti] = 0–5000, 2 bar ethylene/hydrogen (98:2), 50 mL hexanes, 30 minutes, and 60 °C.

Table S5 Melting temperature and crystallinity (relative to $\Delta_m H$ = 293 J g^{-1})[26] of polyethylene produced by **1**$_{sMAO}$/TIBA in the presence of 2% hydrogen as a function of T_p.

T_p /°C	T_m /°C	X_c (%)
50	134.5	117.0
60	133.5	93.6
70	134.7	109.8
80	134.2	119.9
90	136.0	111.5

3.1.2 Gel-permeation chromatography

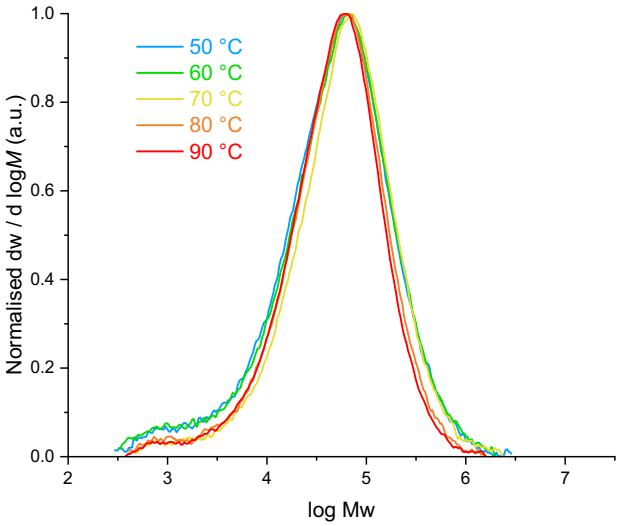

Figure S26 Gel-permeation chromatograms of polyethylene produced by **1**$_{sMAO}$/TIBA as a function of temperature. Polymerization conditions: 10 mg catalyst, 50 mL hexanes, 30 minutes, 150 mg TIBA, and 2 bar ethylene/hydrogen (98:2).

3.2 Diethylzinc

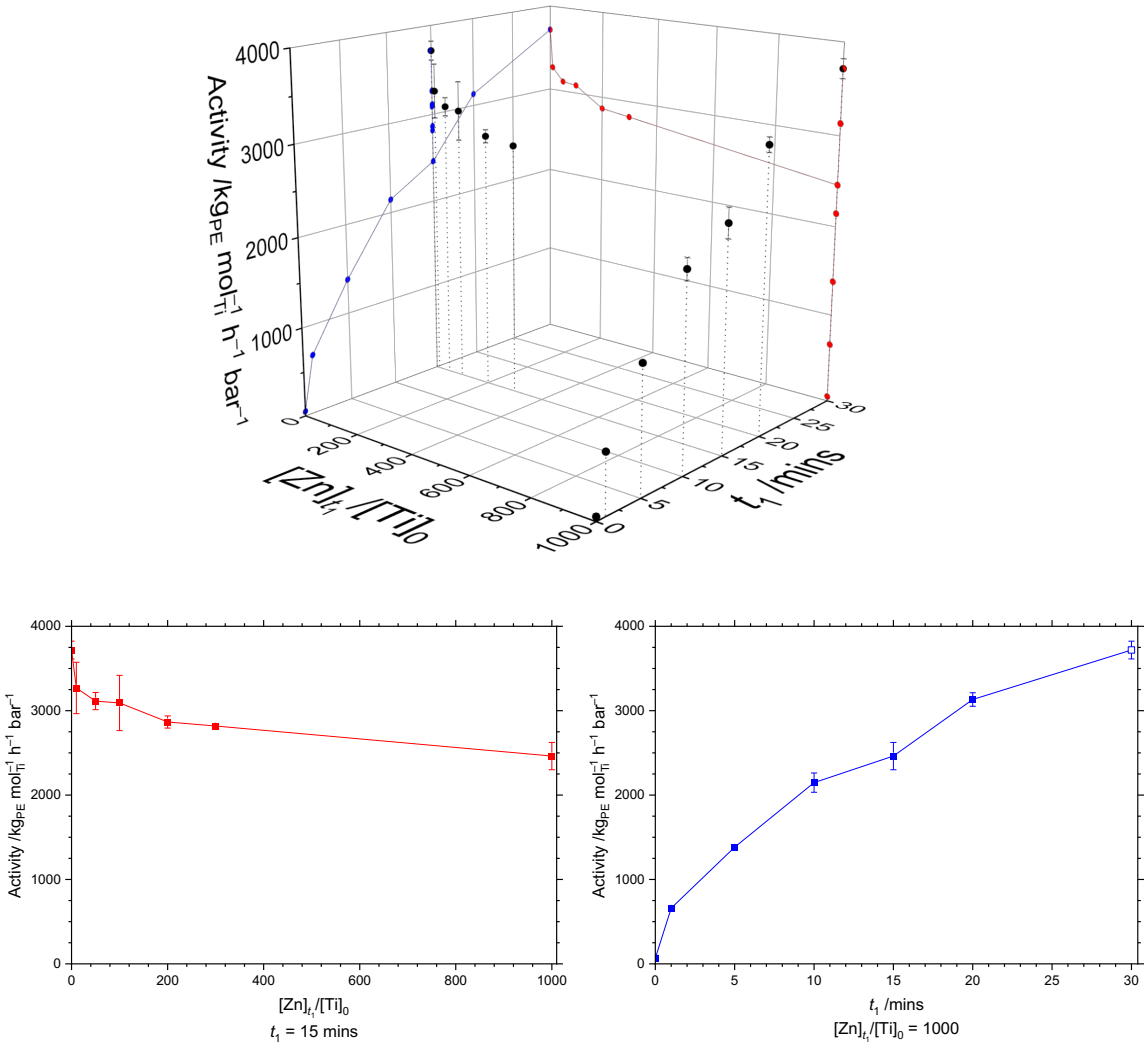

Figure S27 Slurry-phase polymerization activity of **1**$_{sMAO}$/TIBA/$ZnEt_2$ as a function of $[Zn]_{t_1}/[Ti]_0$. Polymerisation conditions: 10 mg catalyst, 150 mg TIBA, 2 bar ethylene, 50 mL hexanes, 30 minutes, and 60 °C.

3.2.1 Gel-permeation chromatography

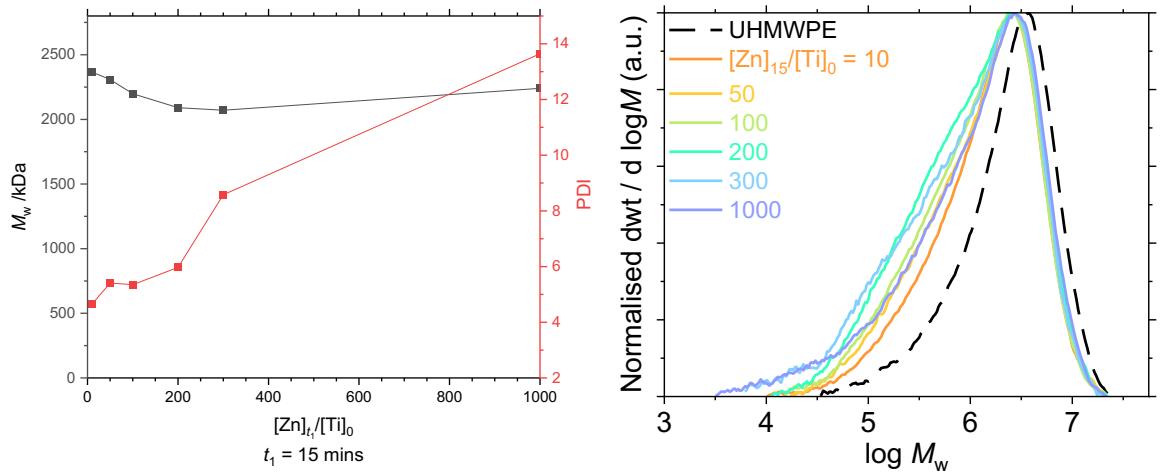

Figure S28 Weight-average molecular weight and dispersity (left) and gel-permeation chromatograms (right) of polyethylene synthesised by **1**$_{sMAO}$/TIBA/ZnEt$_2$ as a function of [Zn]$_{t1}$/[Ti]$_0$ at t_1 = 15 minutes.

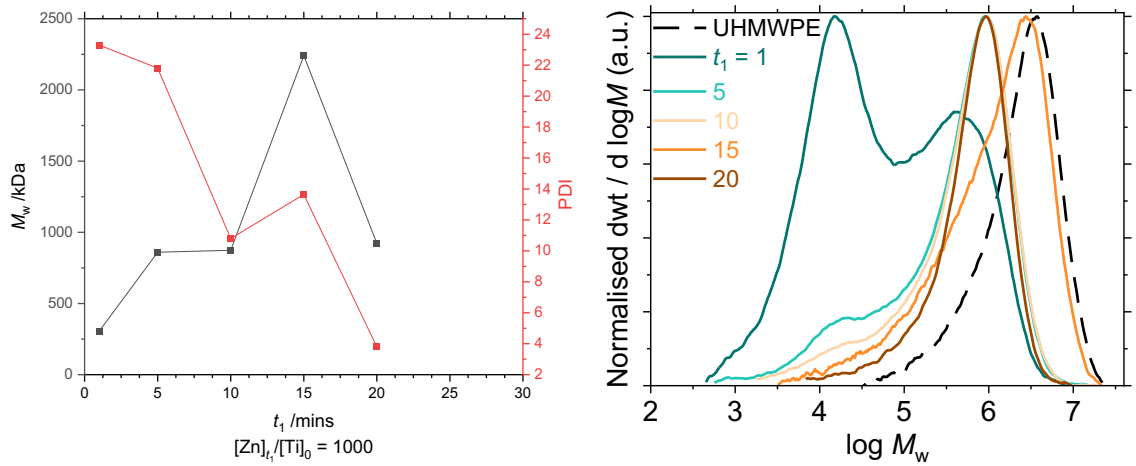

Figure S29 Weight-average molecular weight and dispersity (left) and gel-permeation chromatograms (right) of polyethylene synthesised by **1**$_{sMAO}$/TIBA/ZnEt$_2$ as a function of t_1 at [Zn]$_{t1}$/[Ti]$_0$ = 1000.

3.2.2 Rheology

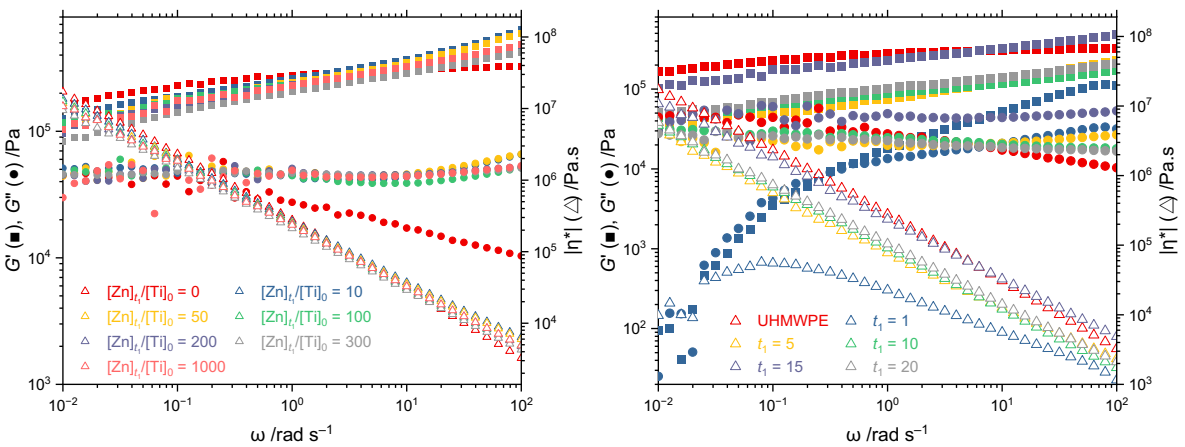

Figure S30 Rheological storage and loss moduli and complex viscosity of polyethylene synthesised by **1**$_{sMAO}$/TIBA/ZnEt$_2$ as a function of [Zn]$_{t1}$/[Ti]$_0$ (left; t_1 = 15 minutes) and t_1 (right; [Zn]$_{t1}$/[Ti]$_0$ = 1000).

3.2.3 Differential scanning calorimetry

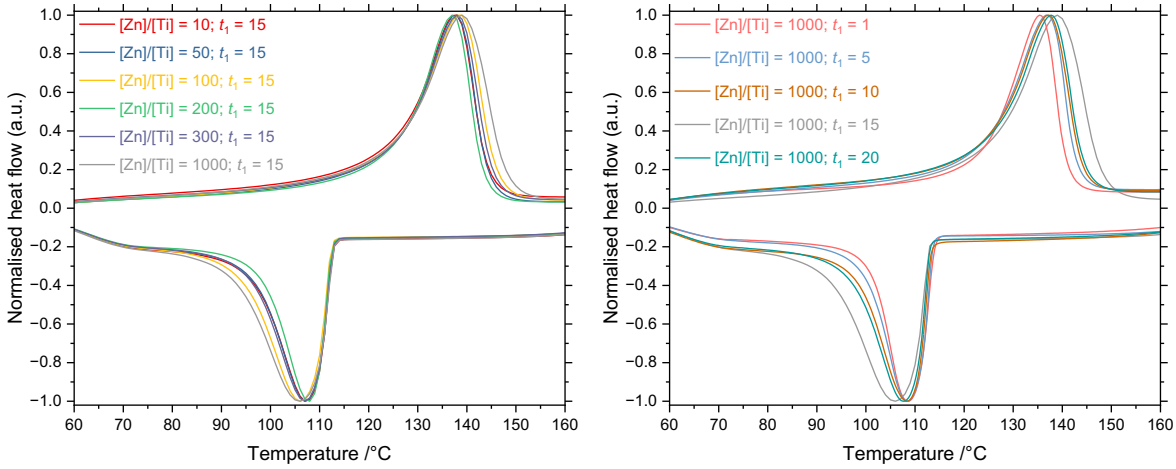

Figure S31 Differential scanning calorimetry plots (20 K min^{-1}; second cycle) of polyethylene synthesised by **1**$_{\mathbf{sMAO}}$/TIBA/ZnEt$_2$ as a function of [Zn]$_{t_1}$/[Ti]$_0$. Polymerisation conditions: 10 mg catalyst, 150 mg TIBA, 2 bar ethylene, 50 mL hexanes, 30 minutes, and 60 °C.

Table S6 Melting point and crystallinity (relative to $\Delta_m H$ = 293 J g^{-1})[26] of polyethylene produced by **1**$_{\mathbf{sMAO}}$/TIBA/ZnEt$_2$ as a function of [Zn]$_{t_1}$/[Ti]$_0$.

[Zn]$_{t_1}$/[Ti]$_0$	t_1 /minutes	T_m /°C	X_c (%)
10	15	137.7	75.4
50	15	137.8	70.6
100	15	138.7	72.4
200	15	137.2	73.0
300	15	138.0	78.3
1000	1	135.5	110.7
1000	5	137.0	91.2
1000	10	137.2	89.1
1000	15	139.0	82.2
1000	20	137.7	80.4

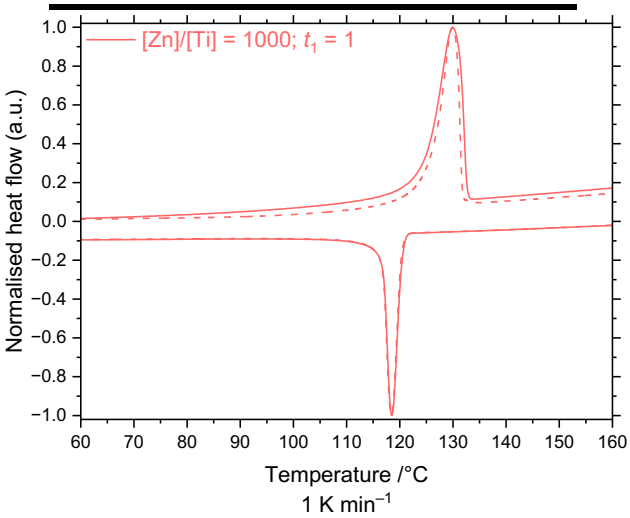

Figure S32 Differential scanning calorimetry plots (1 K min^{-1}; first cycle dashed, second cycle solid) of polyethylene synthesised by **1**$_{\mathbf{sMAO}}$/TIBA/ZnEt$_2$. Polymerisation conditions: 10 mg catalyst, 150 mg TIBA, [Zn]$_{t_1}$/[Ti]$_0$, t_1 = 1 minute, 2 bar ethylene, 50 mL hexanes, 30 minutes, and 60 °C.

4 Multisite catalysts for bimodal polyethylene

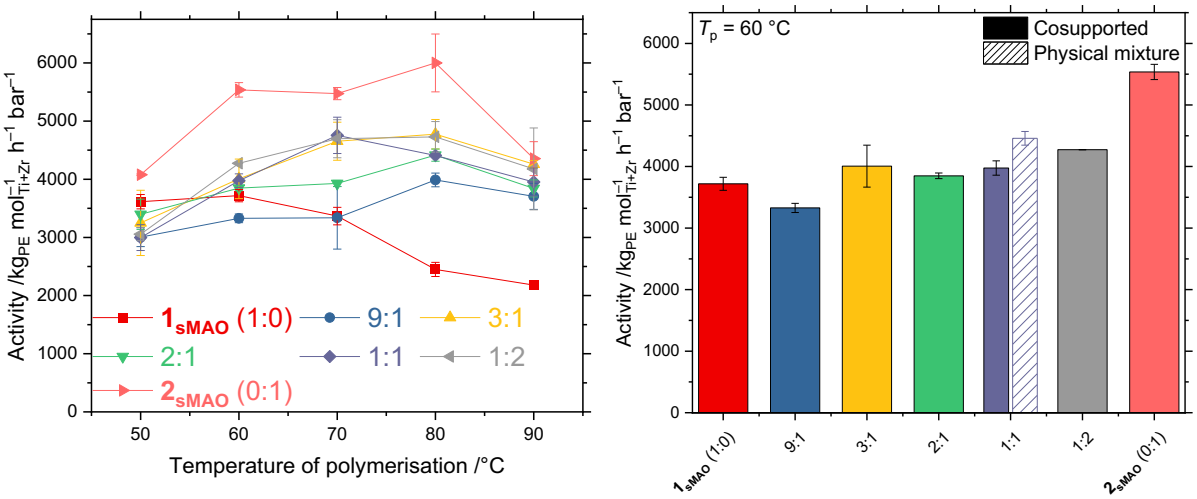

Figure S33 Slurry-phase ethylene polymerization activity of multisite catalysts immobilised on sMAO.

4.1 Differential scanning calorimetry

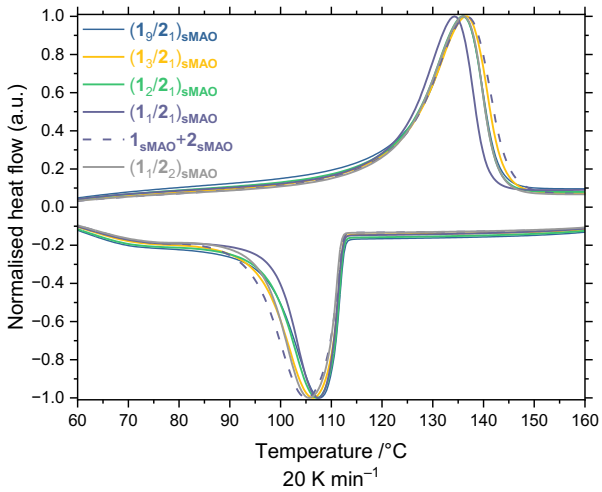

Figure S34 Differential scanning calorimetry plot (20 K min^{-1}; second cycle) of polyethylene produced by $(\mathbf{1}/\mathbf{2})_{sMAO}$/TIBA as a function of [Ti]/[Zr]. Polymerisation conditions: $[Al_{sMAO}]/[Ti+Zr]_0$ = 200, 10 mg catalyst, 150 mg TIBA, 2 bar ethylene, 50 mL hexanes, 30 minutes, and 60 °C.

Table S7 Melting point and crystallinity (relative to $\Delta_m H$ = 293 J g^{-1})[26] of polyethylene produced by $(\mathbf{1}/\mathbf{2})_{sMAO}$/TIBA as a function of [Ti]/[Zr] at T_p = 60 °C.

Catalyst	T_m /°C	X_c (%)
$(\mathbf{1}_9/\mathbf{2}_1)_{sMAO}$	136.0	81.9
$(\mathbf{1}_3/\mathbf{2}_1)_{sMAO}$	136.5	86.6
$(\mathbf{1}_2/\mathbf{2}_1)_{sMAO}$	136.1	84.4
$(\mathbf{1}_1/\mathbf{2}_1)_{sMAO}$	134.4	96.2
$\mathbf{1}_{sMAO}+\mathbf{2}_{sMAO}$	136.7	97.1
$(\mathbf{1}_1/\mathbf{2}_2)_{sMAO}$	135.9	92.6

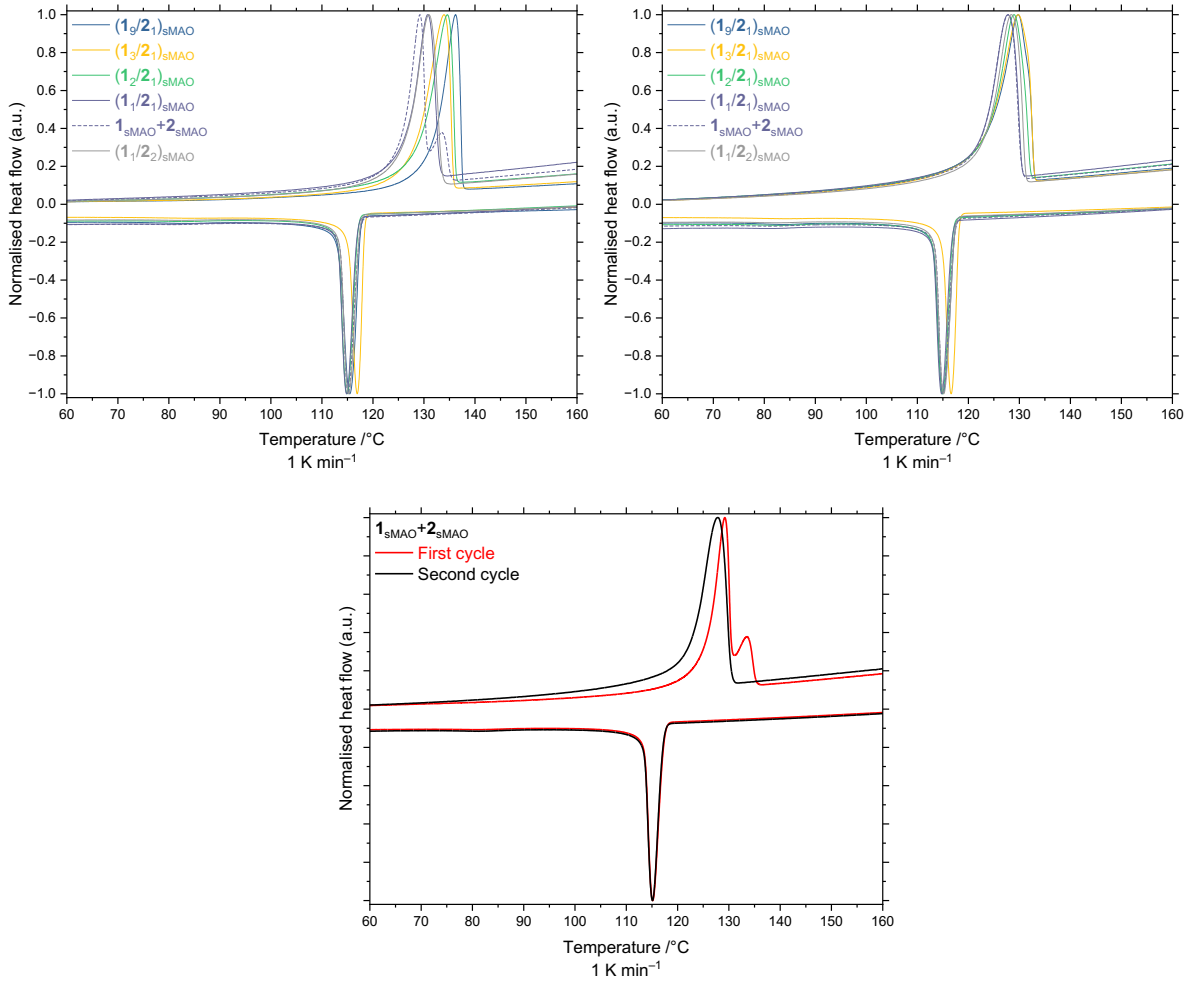

Figure S35 Differential scanning calorimetry plot (1 K min^{-1}; above left: first cycle, above right: second cycle) of polyethylene produced by (**1**/**2**)$_{\mathbf{sMAO}}$/TIBA and **1**$_{\mathbf{sMAO}}$+**2**$_{\mathbf{sMAO}}$/TIBA as a function of [Ti]/[Zr]. Polymerisation conditions: [Al$_{sMAO}$]/[Ti+Zr]$_0$ = 200, 10 mg catalyst, 150 mg TIBA, 2 bar ethylene, 50 mL hexanes, 30 minutes, and 60 °C. (Below) The observation of two melting peaks in the first cycle of the polymer produced by the physical mixture catalyst is consistent with the formation of separate HDPE and UHMWPE particles, whereas the single thermal phase resulting from the coimmobilised catalysts suggests homogeneous nanostructured polymer alloys.

4.2 Gel-permeation chromatography

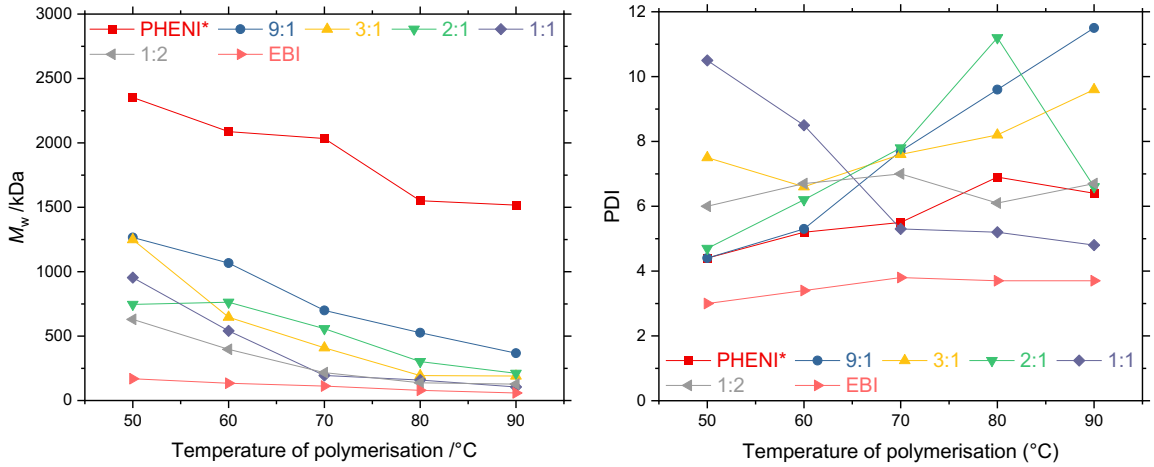

Figure S36 Weight-average molecular weight (left) and dispersity (right) of polyethylene synthesised by multisite catalysts $(\mathbf{1/2})_{\mathbf{sMAO}}$ as a function of Ti:Zr and temperature of polymerization.

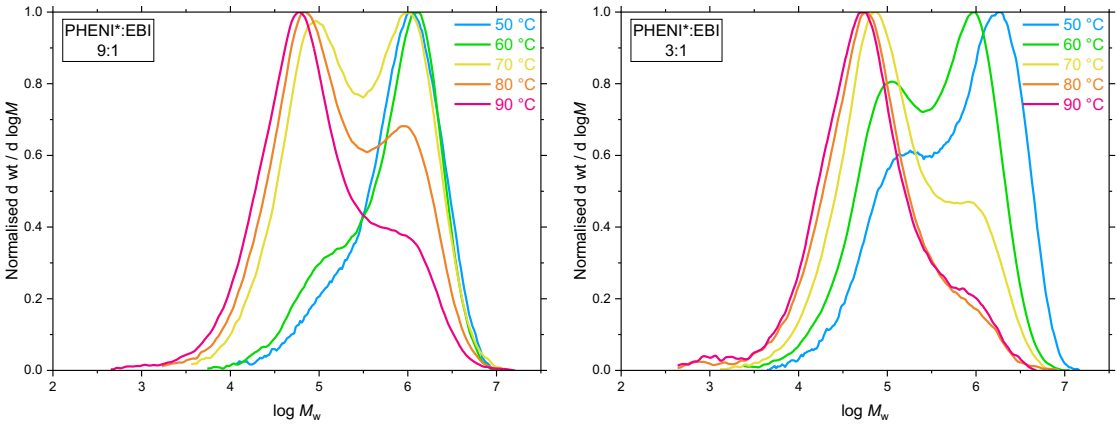

Figure S37 Gel-permeation chromatograms of polyethylene produced by $(\mathbf{1/2})_{\mathbf{sMAO}}$ (9:1 (left) and 3:1 (right)) as a function of temperature of polymerization.

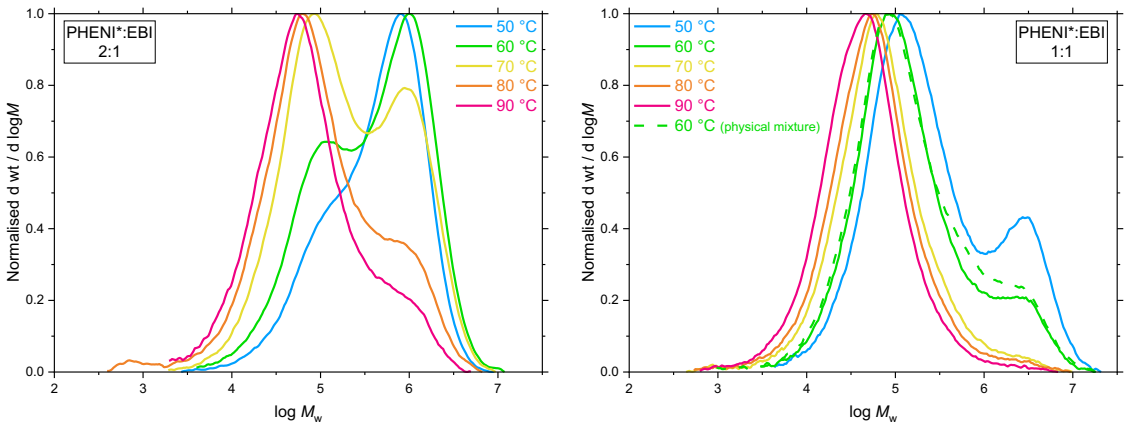

Figure S38 Gel-permeation chromatograms of polyethylene produced by $(\mathbf{1/2})_{\mathbf{sMAO}}$ (2:1 (left) and 1:1 (right; including $\mathbf{1}_{\mathbf{sMAO}}/\mathbf{2}_{\mathbf{sMAO}}$)) as a function of temperature of polymerization.

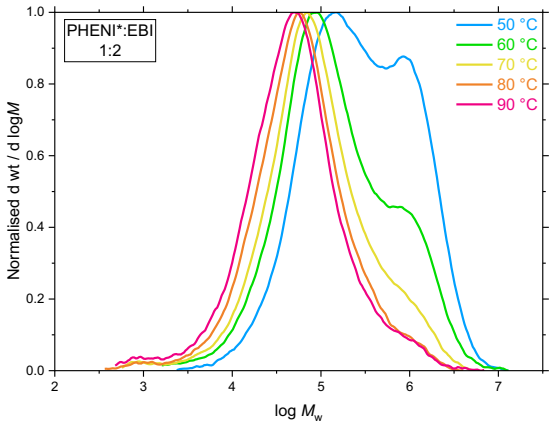

Figure S39 Gel-permeation chromatograms of polyethylene produced by (**1**/**2**)$_{sMAO}$ (1:2) as a function of temperature of polymerization.

Table S8 Deconvolution of gel-permeation chromatograms of polyethylene produced by (**1**/**2**)$_{sMAO}$ or **1**$_{sMAO}$/**2**$_{sMAO}$ as a function of [Ti]/[Zr] and T_p.

		Total GPC		Low M_w fraction (<5.5 Log$M$)		High M_w fraction (>5.5 Log$M$)		
Ti:Zr	**T_p /°C**	**M_w /kDa**	***Đ***	**M_w /kDa**	***Đ***	**M_w /kDa**	***Đ***	**Mass fraction (wt%)**
9:1	50	1266	4.4	136	1.8	1567	1.7	78.2
	60	1067	5.3	122	1.9	1431	1.6	71.4
	70	699.7	7.7	100	2.1	1352	1.6	47.1
	80	526.5	9.6	85.9	2.4	1311	1.7	35.2
	90	367.2	11.5	74.5	3.2	1195	1.6	25.3
3:1	50	1249	7.5	121	1.9	1832	1.9	64.3
	60	647.3	6.6	109	2.0	1147	1.6	49.9
	70	409.0	7.6	88.7	2.2	1119	1.6	29.6
	80	193.5	8.2	72.6	2.3	898	1.5	13.7
	90	190.0	9.6	68.0	2.3	884	1.5	14.1
2:1	50	746.5	4.7	122	1.9	1073	1.5	61.4
	60	763.0	6.2	112	2.0	1222	1.6	55.2
	70	558.1	7.8	96.4	2.1	1201	1.6	39.0
	80	302.4	11.2	79.0	2.2	1006	1.6	21.8
	90	211.4	6.6	69.7	2.3	901	1.5	15.0
				(<6.0 Log$M$)		(>6.0 Log$M$)		
1:1	50	948.0	10.8	206	2.9	3391	1.5	22.2
	60	531.3	8.6	167	2.9	3005	1.4	12.4
	70	194.7	6.1	113	3.0	2331	1.3	3.0
	80	158.7	5.4	95.5	3.2	2463	1.4	2.3
	90	105.1	4.9	76.3	3.3	2181	1.3	1.3
1+1	60	543.0	8.8	173	3.2	2848	1.4	12.9
				(<5.5 Log$M$)		(>5.5 Log$M$)		
1:2	50	629.9	6.0	129	2.0	1249	1.6	44.8
	60	396.9	6.7	103	2.3	1142	1.5	28.3
	70	216.2	7.0	88.2	2.4	934	1.4	15.4
	80	137.6	6.1	74.8	2.5	787	1.3	9.0
	90	127.2	6.7	67.1	2.5	862	1.4	7.8

4.3 Mechanical analysis

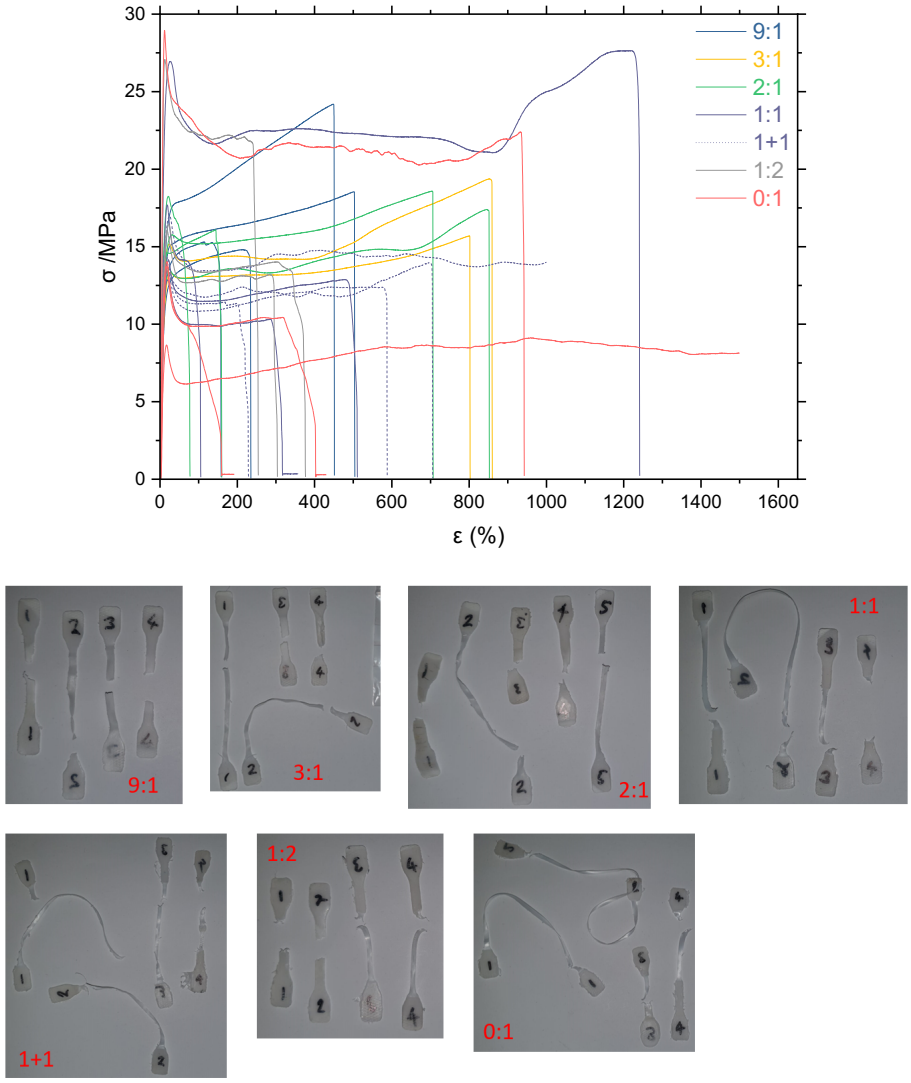

Figure S40 Engineering stress-strain tensile curves for PE synthesised by multisite catalysts at 60 °C.

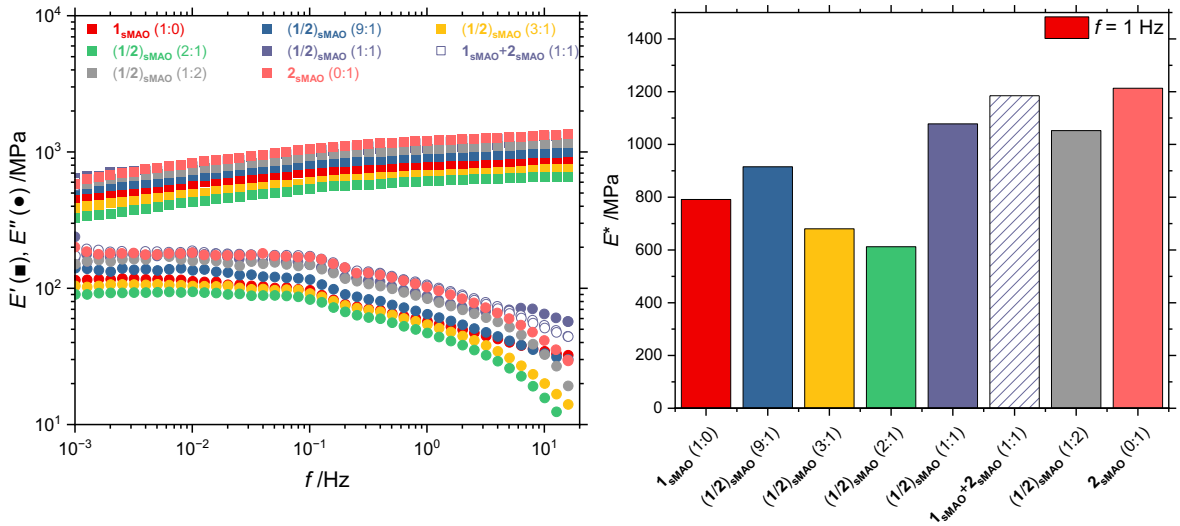

Figure S41 Dynamic mechanical analysis of polyethylene synthesised by multisite catalysts at T_p = 60 °C as a function of Ti:Zr. $E^* = |E' + iE''|$.

4.4 Rheology

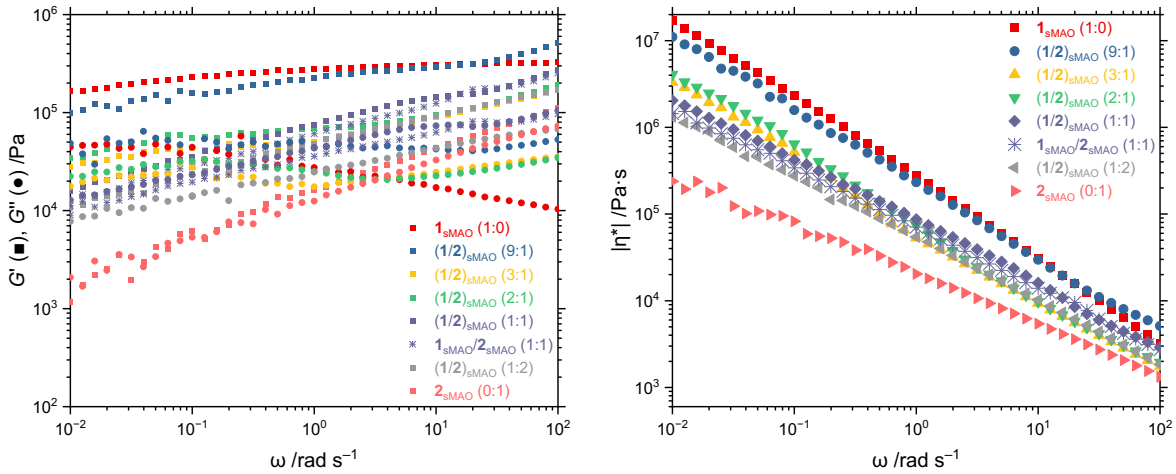

Figure S42 Rheological storage and loss moduli (left) and complex viscosity (right) of polyethylene synthesised by multisite catalysts at T_p = 60 °C as a function of angular frequency, measured at 160 °C.

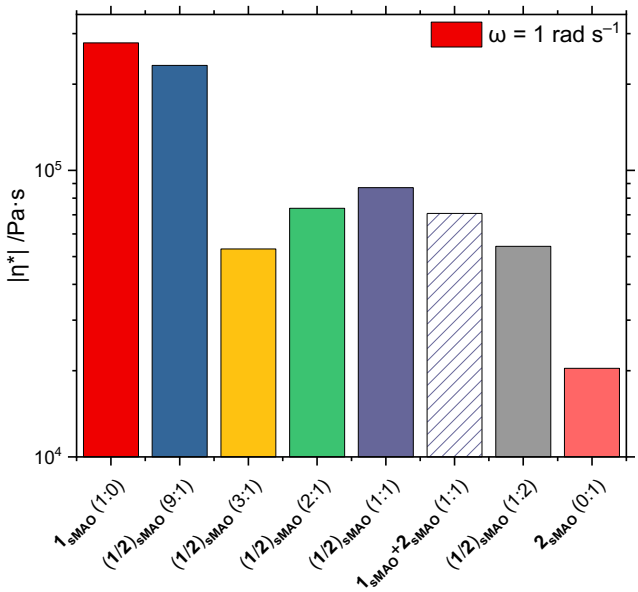

Figure S43 Complex viscosity (measured at 160 °C, ω = 1 rad s^{-1}) of polyethylene synthesised by multisite catalysts at T_p = 60 °C.

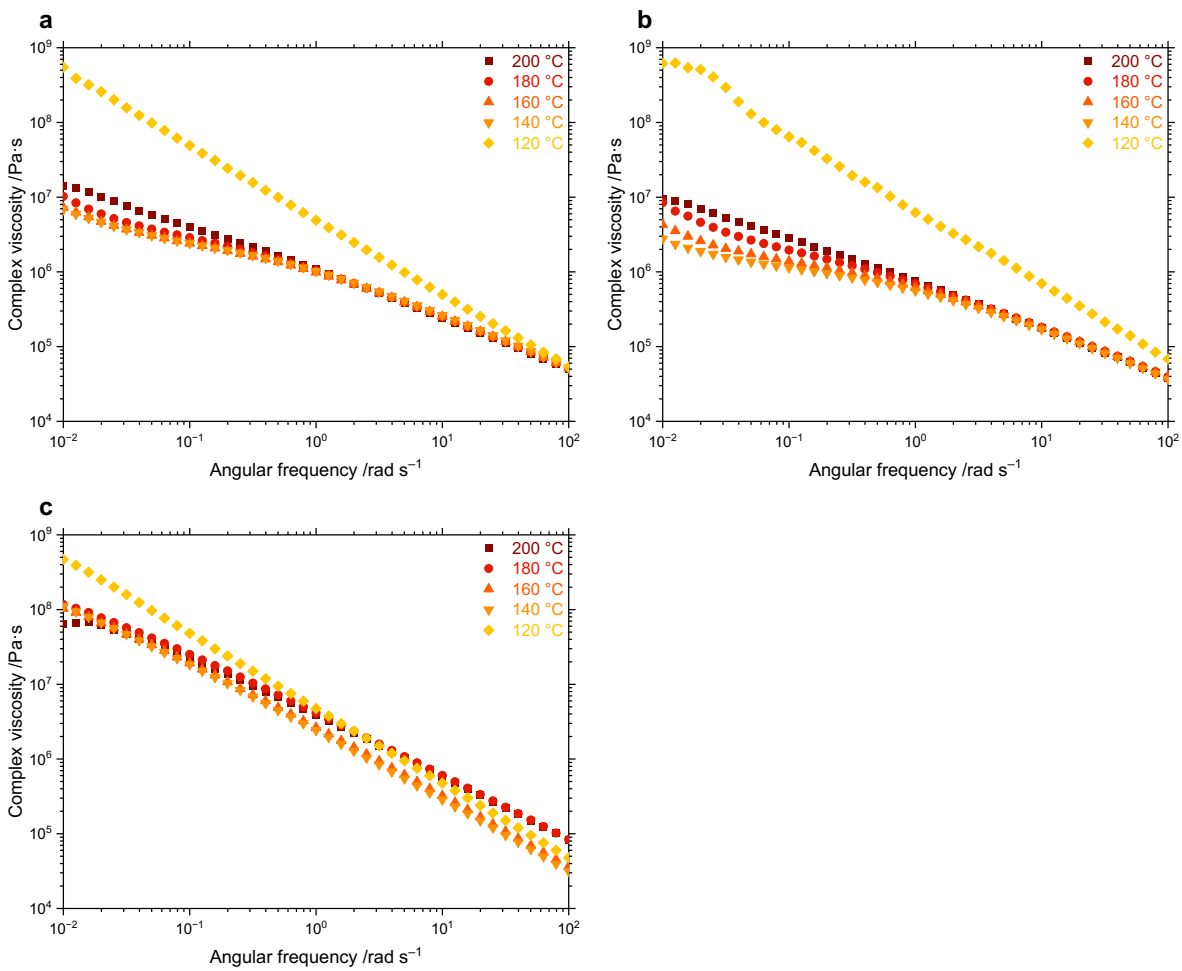

Figure S44 Complex viscosity (Time-Temperature Superposition 120–200 °C, 10^{-2}–10^{2} rad s^{-1}) of polyethylene synthesised by multisite catalysts (a $(\mathbf{1}_1/\mathbf{2}_1)_{sMAO}$; b $\mathbf{1}_{sMAO}$+$\mathbf{2}_{sMAO}$; c $(\mathbf{1}_3/\mathbf{2}_1)_{sMAO}$) at T_p = 60 °C.

5 Polyethylene-polyethylene composite blends

5.1 Microcompounding, film extrusion

Table S9 Polyethylene-polyethylene blends prepared by microcompounding UHMWPE with either LDPE or HDPE. In both cases, up to 30 wt% could be achieved.

	LDPE		**HDPE**	
UHMWPE	Thickness /µm	Image	Thickness /µm	Image
0 wt%	50–150		60–180	
10 wt%	150–300		250–500	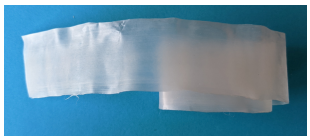
15 wt%	100–400		80–250	
20 wt%	250–500		150–400	
30 wt%	300–550	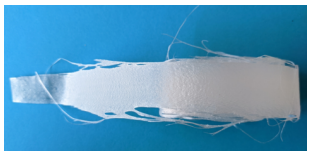	150–190	

5.2 PE/UHMWPE characterisation

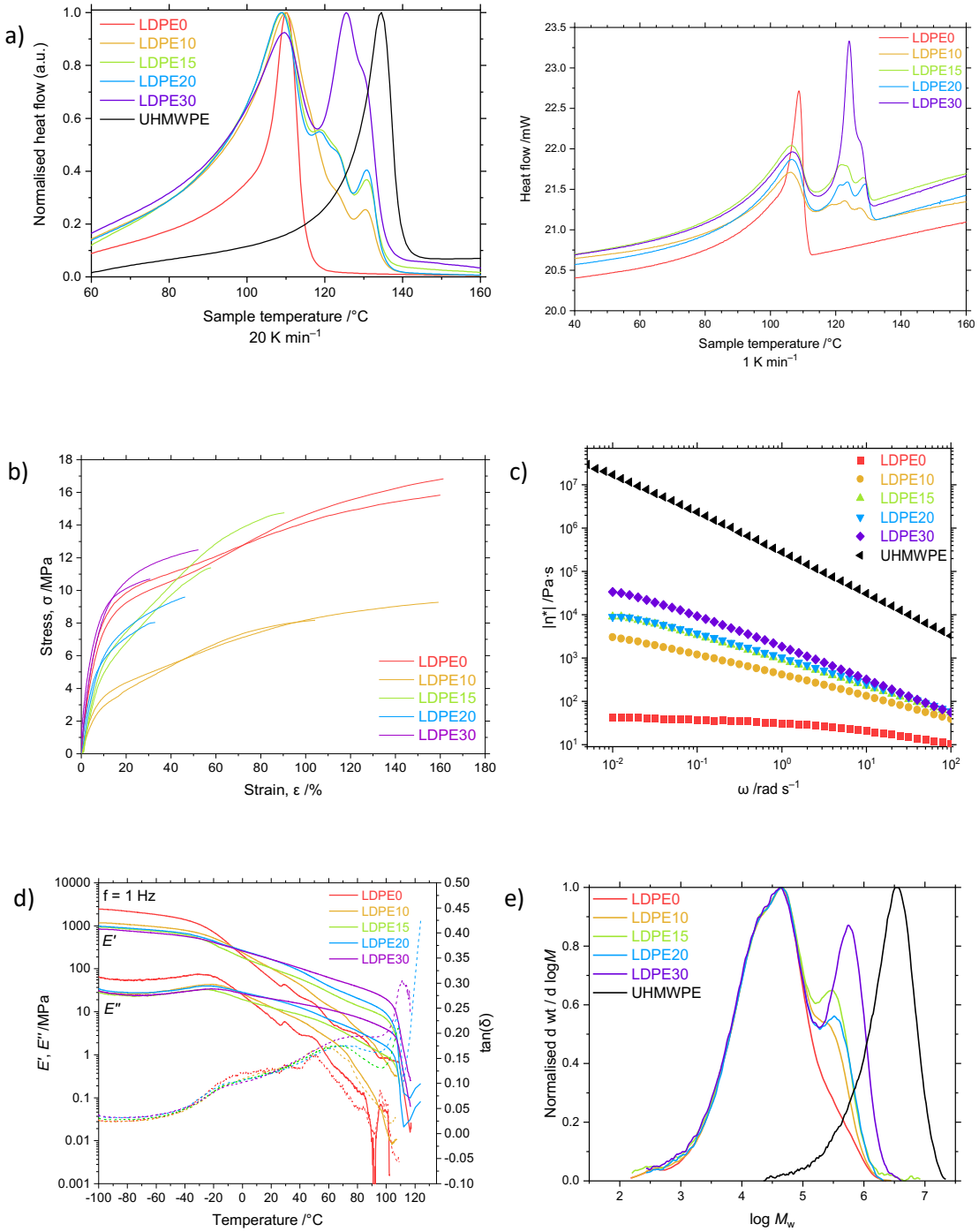

f)

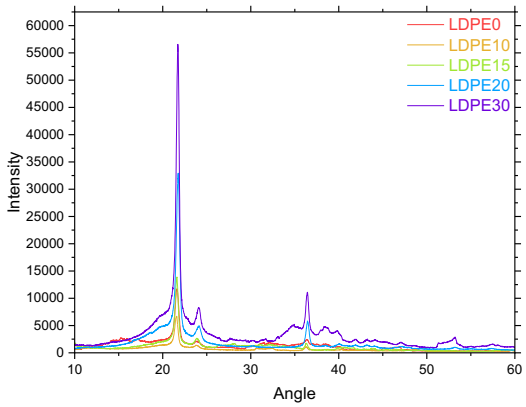

Figure S45 a) DSC thermograms (at 20 K min^{-1} and 1 K min^{-1}), b) engineering stress-strain curves, c) rheological frequency sweep, d) DMTA, e) gel-permeation chromatograms, and f) wide-angle X-ray scattering of LDPE/UHMWPE blends across a composition range of 0–30 wt% UHMWPE.

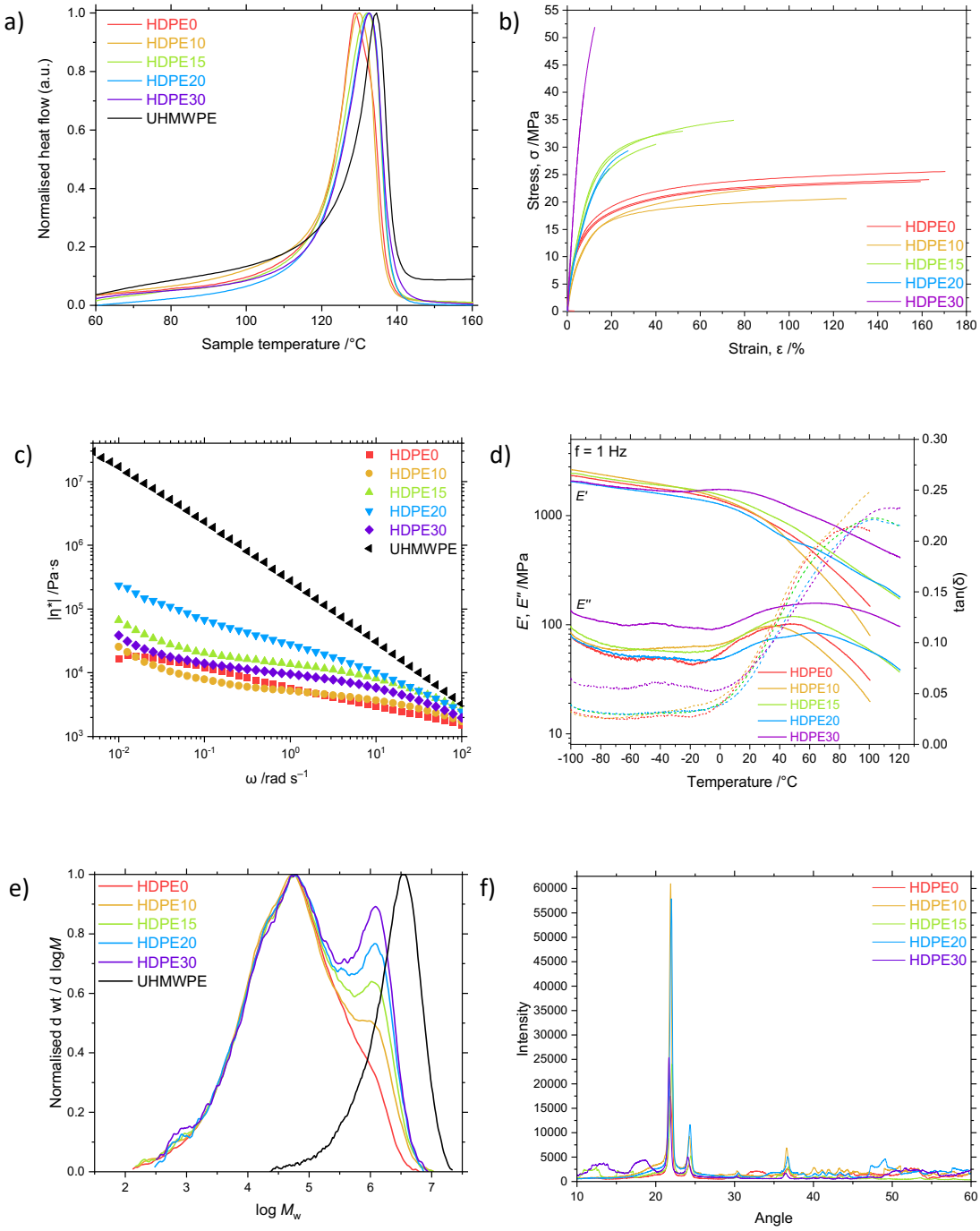

Figure S46 a) DSC thermograms, b) engineering stress-strain curves, c) rheological frequency sweep, d) DMTA, e) gel-permeation chromatograms, and f) wide-angle X-ray scattering of HDPE/UHMWPE blends across a composition range of 0–30 wt% UHMWPE.

Table S10 Deconvolution of gel-permeation chromatograms of PE/UHMWPE blends.

		Total GPC		Low M_w fraction (<5.25 Log$M$)		High M_w fraction (>5.25 Log$M$)		
Matrix	**UHMWPE (wt%)**	**M_w /kDa**	**Đ**	**M_w /kDa**	**Đ**	**M_w /kDa**	**Đ**	**Mass fraction (wt%)**
LDPE	0	84.3	10.7					
	10	108.6	13.1	42.3	5.7	417.3	1.3	17.2
	15	125.4	14.8	42.8	4.4	452.4	1.3	20.9
	20	122.3	11.4	43.4	4.5	457.1	1.3	20.2
	30	234.1	20.7	41.4	4.4	625.2	1.4	30.4
				<5.5 Log$M$		>5.5 Log$M$		
HDPE	0	217.4	26.1					
	10	331.9	38.4	68.3	10.4	1231	1.6	22.9
	15	396.4	47.7	70.7	11.7	1294	1.6	26.8
	20	431.3	37.8	71.2	10.8	1290	1.6	29.6
	30	475.3	39.9	72.7	11.7	1326	1.6	32.3

Table S11 Crystallinity of LDPE/UHMWPE and HDPE/UHMWPE blends determined by wide-angle X-ray scattering by Lorentz fitting of the [110] and [200] peaks compared to integrating diffraction pattern between $10 \leq 2\theta/° \leq 29$.

Sample	**Crystallinity (WAXS)**
LDPE0	29.4%
LDPE10	31.1%
LDPE15	37.3%
LDPE20	49.9%
LDPE30	49.2%
HDPE0	49.7%
HDPE10	57.2%
HDPE15	45.7%
HDPE20	62.7%
HDPE30	29.5%

5.3 Microscopy

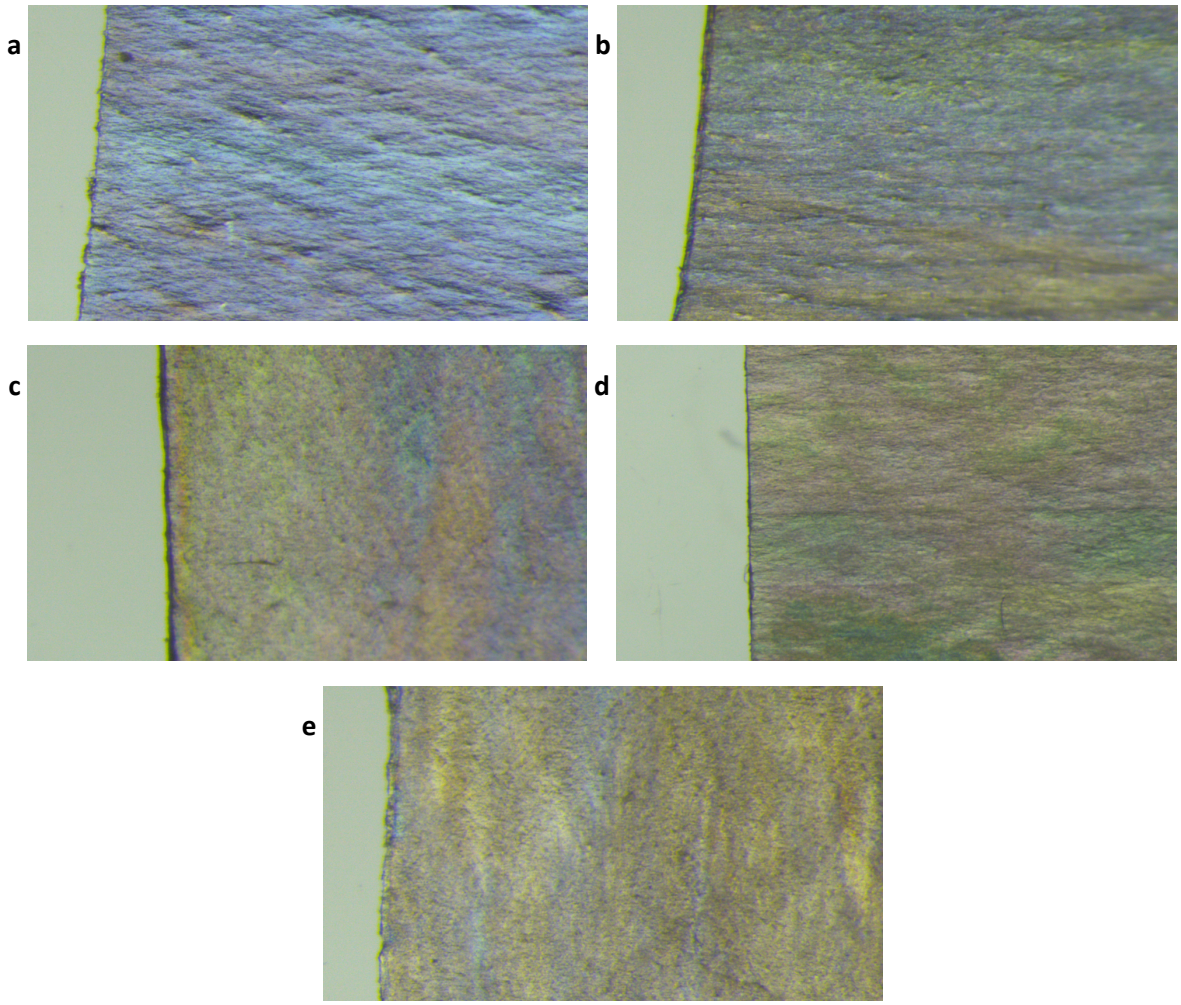

Figure S47 Optical micrographs of HDPE/UHMWPE blends at 2x magnification. **a** HDPE0, **b** HDPE10, **c** HDPE15, **d** HDPE20, **e** HDPE30.

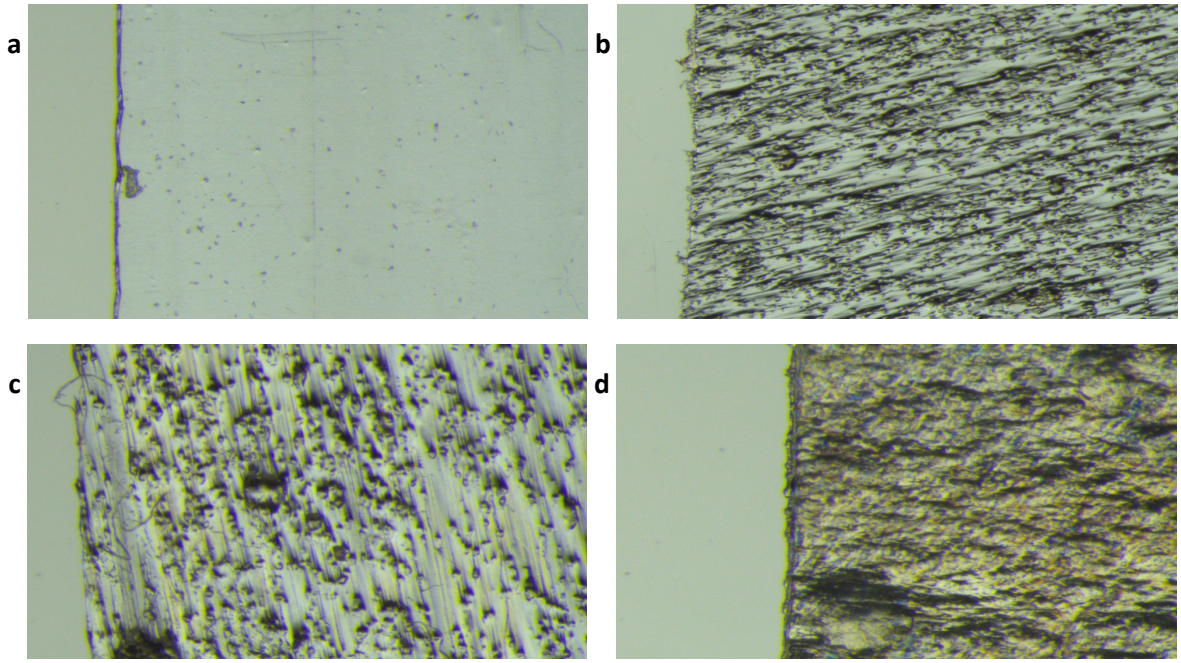

e

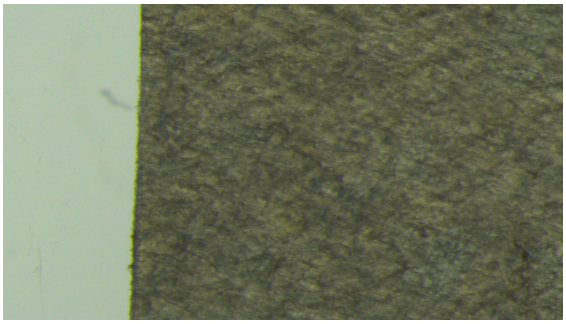

Figure S48 Optical micrographs of LDPE/UHMWPE blends at 2x magnification. **a** LDPE0, **b** LDPE10, **c** LDPE15, **d** LDPE20, **e** LDPE30.

5.4 Scanning Electron Microscopy

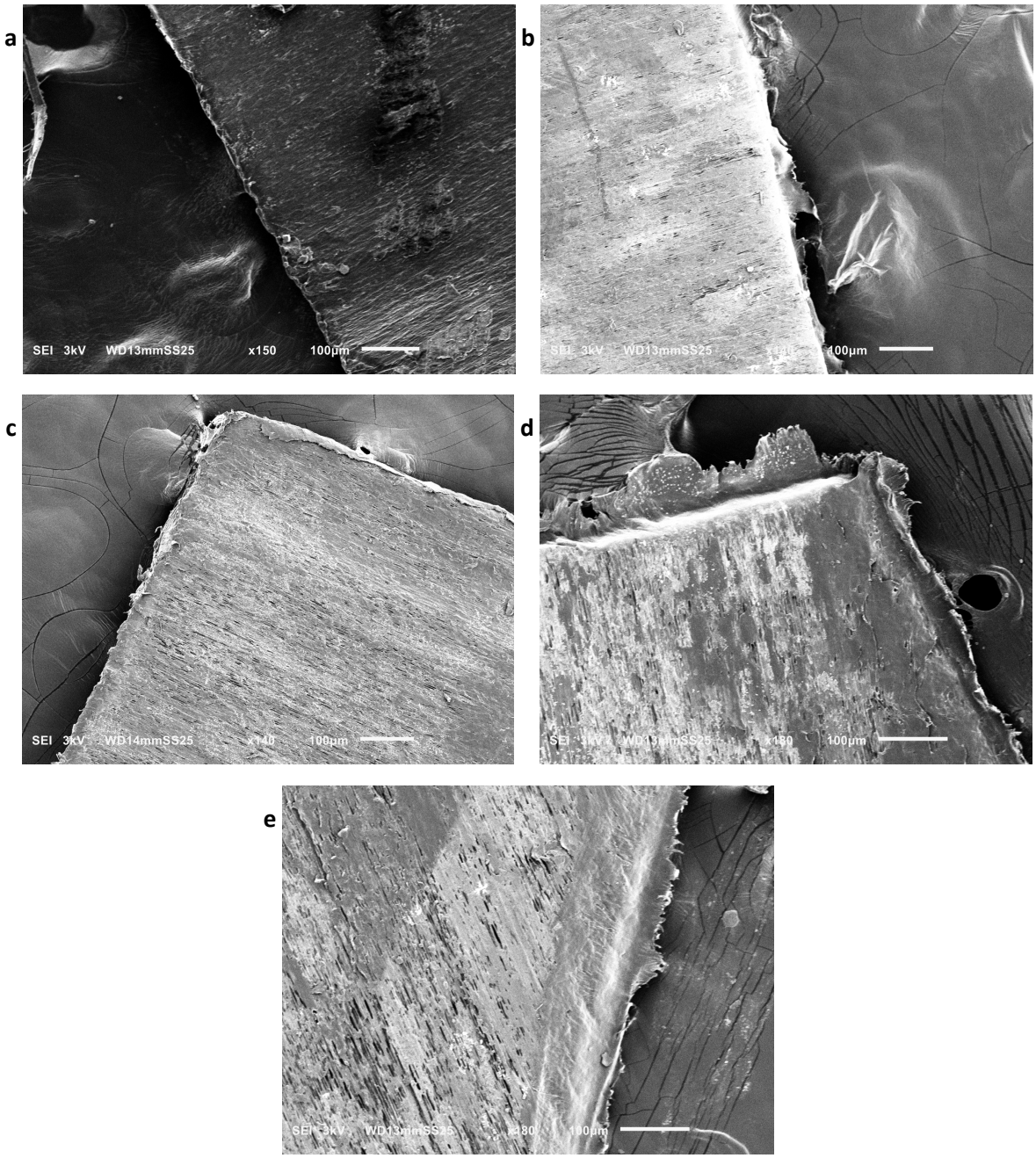

Figure S49 Scanning electron micrographs of HDPE/UHMWPE blends. **a** HDPE0, **b** HDPE10, **c** HDPE15, **d** HDPE20, **e** HDPE30.

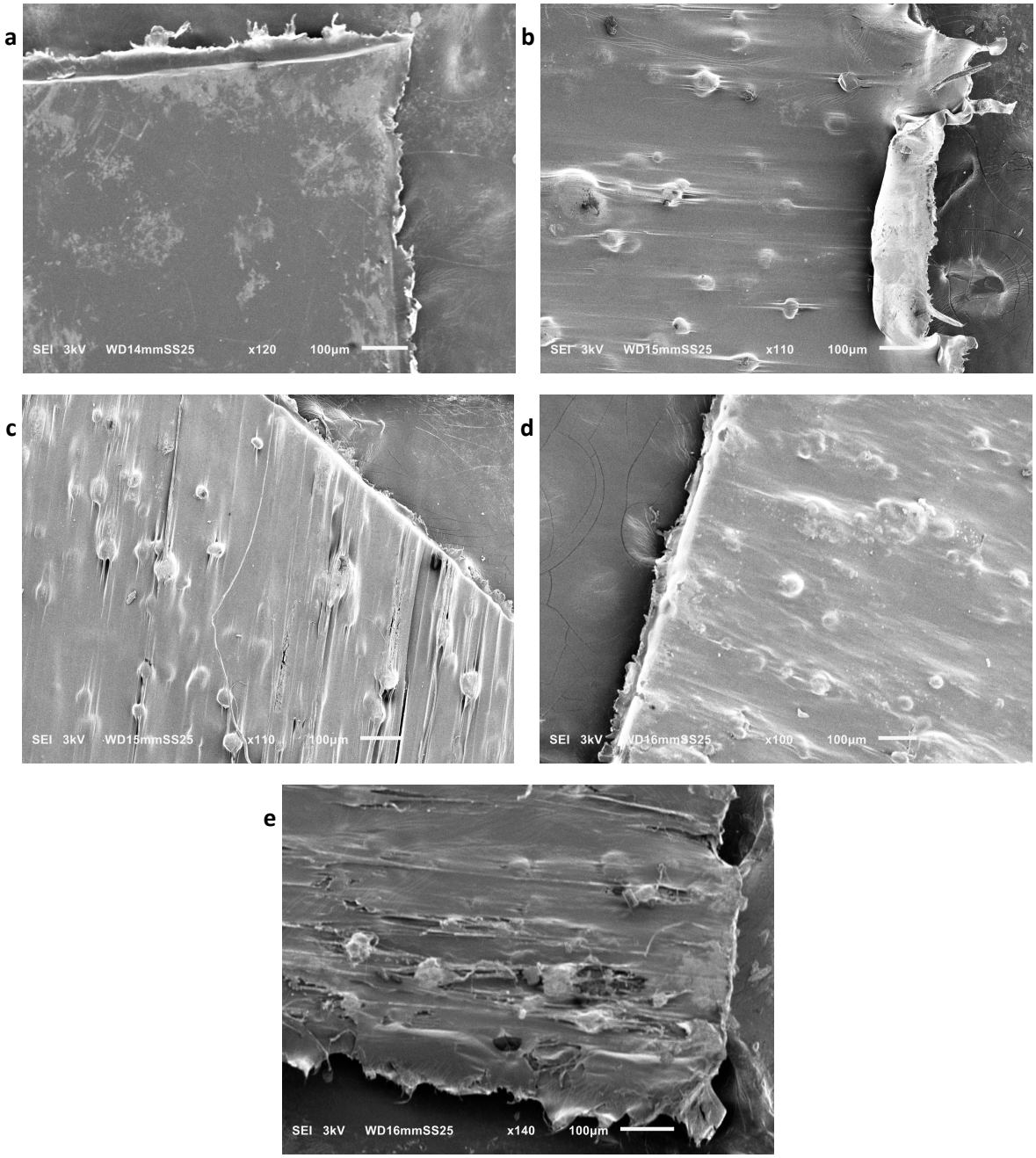

Figure S50 Scanning electron micrographs of LDPE/UHMWPE blends. **a** LDPE0, **b** LDPE10, **c** LDPE15, **d** LDPE20, **e** LDPE30.

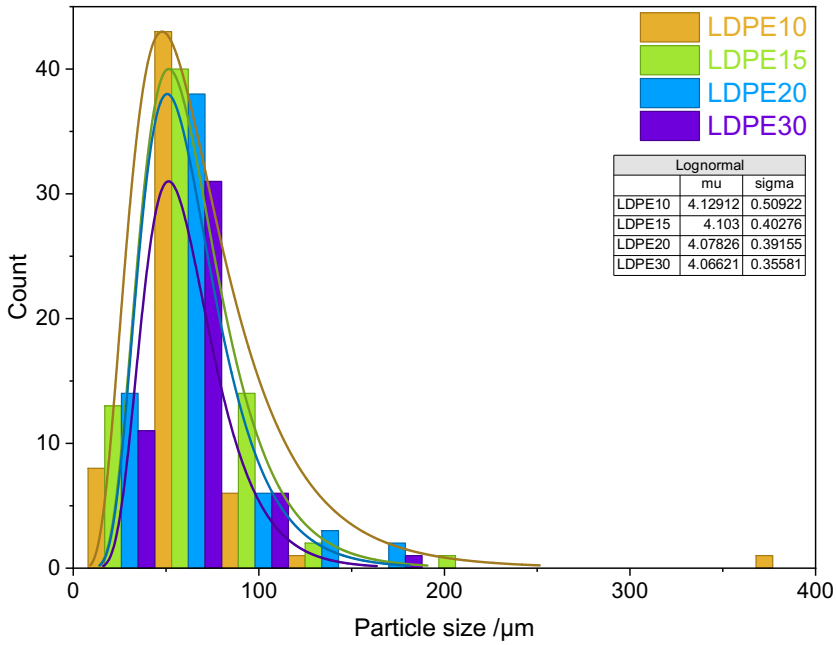

Figure S51 Particle size distribution of UHMWPE particles embedded in the LDPE matrix in LDPE/UHMWPE blends. The distributions are fitted to log-normal curves, $N = 60$ (LDPE10), 70 (LDPE15), 63 (LDPE20), 49 (LDPE30). There is no statistically significant difference between any of the distributions (unpaired *t* test, 0.05 significant threshold).

5.5 Rheometry

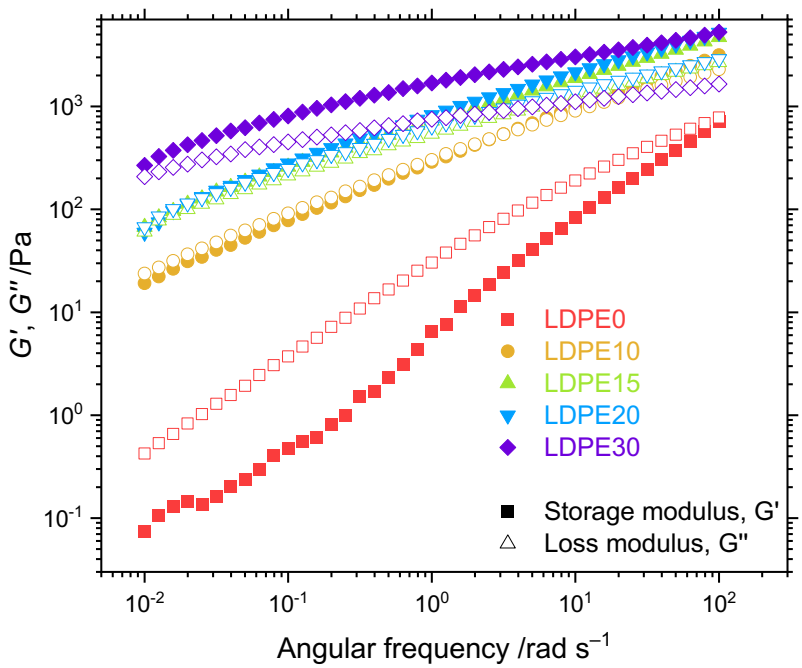

Figure S52 Rheological storage (*G'*, filled) and loss moduli (*G''*, open) as a function of shear angular frequency of LDPE/UHMWPE blends.

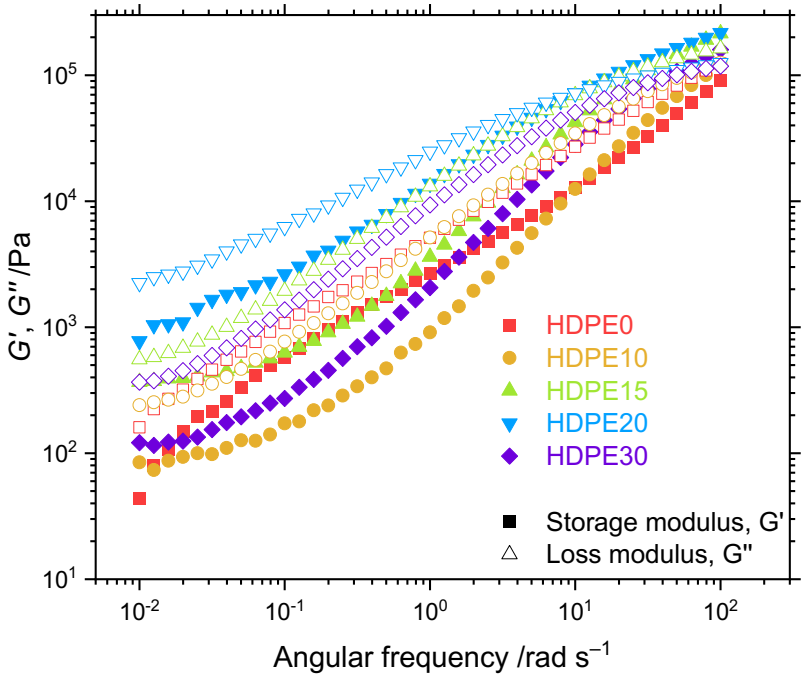

Figure S53 Rheological storage (*G'*, filled) and loss moduli (*G''*, open) as a function of shear angular frequency of HDPE/UHMWPE blends.

5.6 Mixing laws

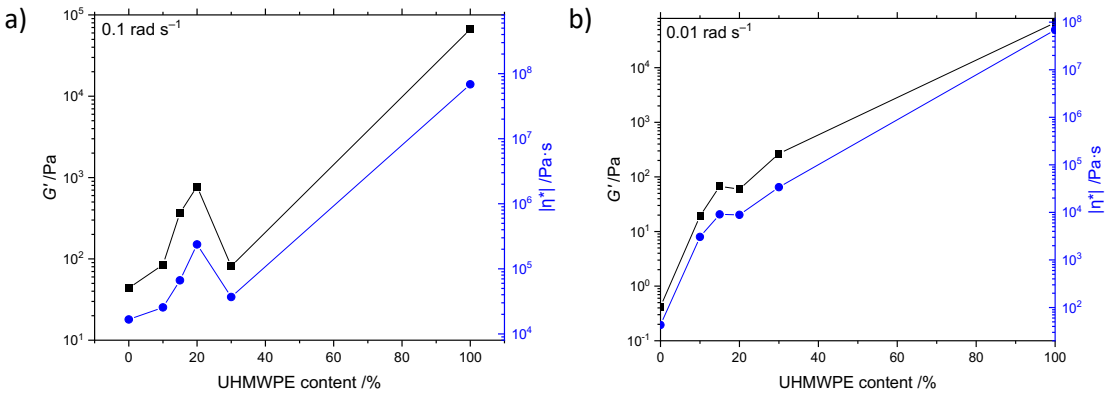

Figure S54 Log-additivity law for rheological parameters, storage modulus *G'* and complex viscosity η*, for a) HDPE/UHMWPE, and b) LDHPE/UHMWPE as a function of polymer blend composition.

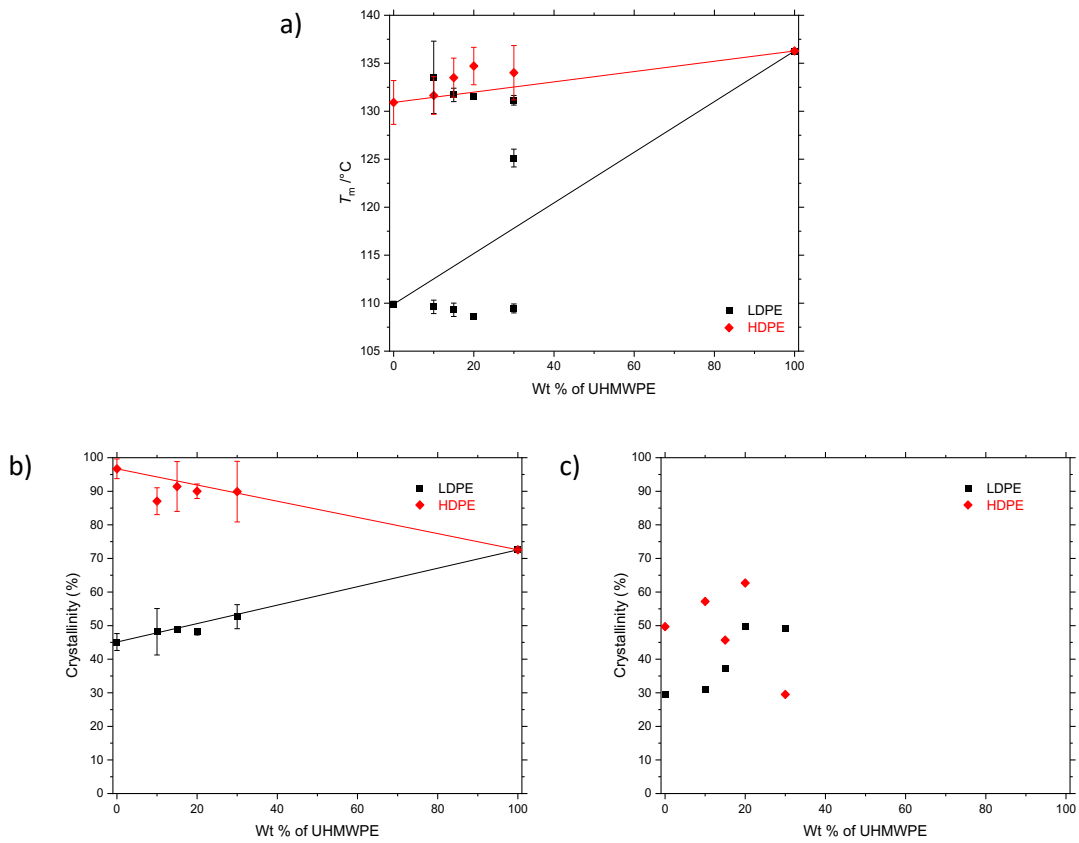

Figure S55 Law of mixtures for a) T_m, b) crystallinity (relative to $\Delta_m H$ = 293 J g^{-1})[26] and c) crystallinity calculated from WAXS of HDPE/UHMWPE and LDPE/UHMWPE as a function of polymer blend composition. Plotted as mean ± standard deviation.

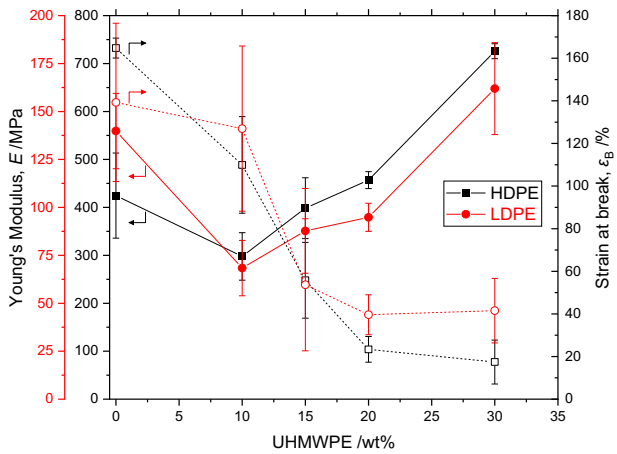

Figure S56 Young's modulus, E, and strain at break, ε_B, of HDPE/UHMWPE and LDPE/UHMWPE as a function of polymer blend composition. Plotted as mean ± standard deviation.

6 References

1 MatWeb.com, *Overview of materials for High Density Polyethylene (HDPE), Ultra High Molecular Weight*, https://www.matweb.com/search/DataSheet.aspx?MatGUID=f9470672aa5549cb9c7b157677d02062, Accessed 5 December, 2022.

2 E. P. C. Mes, H. de Jonge, T. Klein, R. R. Welz, D. T. Gillespie, Characterization of high molecular weight polyethylenes using high temperature asymmetrical flow field-flow fractionation with on-line infrared, light scattering, and viscometry detection, *J. Chromatogr. A*, 2007, **1154**, 319-330.
3 S. Talebi, R. Duchateau, S. Rastogi, J. Kaschta, G. W. M. Peters, P. J. Lemstra, Molar Mass and Molecular Weight Distribution Determination Of UHMWPE Synthesized Using a Living Homogeneous Catalyst, *Macromolecules*, 2010, **43**, 2780-2788.
4 R. P. Gote, D. Mandal, K. Patel, K. Chaudhuri, C. P. Vinod, A. K. Lele, S. H. Chikkali, Judicious Reduction of Supported Ti Catalyst Enables Access to Disentangled Ultrahigh Molecular Weight Polyethylene, *Macromolecules*, 2018, **51**, 4541-4552.
5 N. Makris, The frequency response function of the creep compliance, *Meccanica*, 2019, **54**, 19-31.
6 S. Rastogi, D. Lippits, S. Talebi, B. Wang, Heterogeneous distribution of entanglements in the polymer melt and its influence on crystallization, *Abstr. Pap. Am. Chem. Soc.*, 2007, **234**.
7 D. Romano, N. Tops, E. Andablo-Reyes, S. Ronca, S. Rastogi, Influence of Polymerization Conditions on Melting Kinetics of Low Entangled UHMWPE and Its Implications on Mechanical Properties, *Macromolecules*, 2014, **47**, 4750-4760.
8 G. Forte and S. Ronca, Synthesis of Disentangled Ultra-High Molecular Weight Polyethylene: Influence of Reaction Medium on Material Properties, *Int. J. Polym. Sci.*, 2017, **2017**, 1-8.
9 A. Heidari, H. Zarghami, S. Talebi, M. Rezaei, A disentangled state using TiCl4/MgCl2 catalyst: a case study of polyethylene, *Iran. Polym. J.*, 2018, **27**, 701-708.
10 K. Patel, S. H. Chikkali, S. Sivaram, Ultrahigh molecular weight polyethylene: Catalysis, structure, properties, processing and applications, *Prog. Polym. Sci.*, 2020, **109**, 101290.
11 F. Christakopoulos, E. M. Troisi, A. S. Sologubenko, N. Friederichs, L. Stricker, T. A. Tervoort, Melting kinetics, ultra-drawability and microstructure of nascent ultra-high molecular weight polyethylene powder, *Polymer*, 2021, **222**, 123633.
12 K. Liu, E. L. de Boer, Y. Yao, D. Romano, S. Ronca, S. Rastogi, Heterogeneous Distribution of Entanglements in a Nonequilibrium Polymer Melt of UHMWPE: Influence on Crystallization without and with Graphene Oxide, *Macromolecules*, 2016, **49**, 7497-7509.
13 C. G. Collins Rice, J.-C. Buffet, Z. R. Turner, D. O'Hare, Supported permethylindenyl titanium catalysts for the synthesis of disentangled ultra-high molecular weight polyethylene (disUHMWPE), *Chem. Commun.*, 2021, **57**, 8600-8603.
14 S. Rastogi, D. R. Lippits, G. W. M. Peters, R. Graf, Y. Yao, H. W. Spiess, Heterogeneity in polymer melts from melting of polymer crystals, *Nat. Mater.*, 2005, **4**, 635-641.
15 S. Rastogi, D. R. Lippits, G. W. H. Höhne, B. Mezari, P. C. M. M. Magusin, The role of the amorphous phase in melting of linear UHMW-PE; implications for chain dynamics, *J. Phys.: Condens. Matter*, 2007, **19**, 205122.
16 D. R. Lippits, S. Rastogi, G. W. H. Höhne, B. Mezari, P. C. M. M. Magusin, Heterogeneous Distribution of Entanglements in the Polymer Melt and Its Influence on Crystallization, *Macromolecules*, 2007, **40**, 1004-1010.
17 A. Pandey, Y. Champouret, S. Rastogi, Heterogeneity in the Distribution of Entanglement Density during Polymerization in Disentangled Ultrahigh Molecular Weight Polyethylene, *Macromolecules*, 2011, **44**, 4952-4960.
18 W. Li, Z. Yue, A. Lozovoi, O. Petrov, C. Mattea, S. Stapf, Heterogeneous distribution of chain mobility in nascent UHMWPE in the less entangled state, *J. Polym. Res.*, 2018, **25**, 1-8.
19 V. Litvinov, F. Christakopoulos, P. J. Lemstra, Disentangled Melt of Ultrahigh-Molecular-Weight Polyethylene: Fictitious or Real?, *Macromolecules*, 2024, **57**, 3719-3730.
20 N. Li, Q. Zhang, Q. Yang, Y. Huang, X. Liao, W. Zhao, The dependence time of melting behavior on rheological aspects of disentangled polymer melt: a route to the heterogeneous melt, *J. Polym. Res.*, 2015, **22**, 55.
21 J. D. Ferry, *Viscoelastic properties of polymers*, John Wiley & Sons, 1980.

22 Y. W. Inn and D. C. Rohlfing, Application of creep test to obtain the linear viscoelastic properties at low frequency range for polyethylene melts, *Applied Rheology*, 2012, **22**, 15260.
23 F. Cser, About the Lorentz correction used in interpretation of small-angle X-ray scattering data of semicrystalline polymers, *J. Appl. Polym. Sci.*, 2001, **80**, 358-366.
24 A. J. Ryan, W. Bras, G. R. Mant, G. E. Derbyshire, A direct method to determine the degree of crystallinity and lamellar thickness of polymers: application to polyethylene, *Polymer*, 1994, **35**, 4537-4544.
25 C. G. Collins Rice, J. A. Hayden, A. D. Hawkins, L. J. Morris, Z. R. Turner, J.-C. Buffet, D. O'Hare, Trends in Structure and Ethylene Polymerization Reactivity of Transition-Metal Permethylindenyl-phenoxy (PHENI*) Complexes, *Organometallics*, 2024, **43**, 540-556.
26 B. Wunderlich and G. Czornyj, A study of equilibrium melting of polyethylene, *Macromolecules*, 1977, **10**, 906-913.